Next-Generation IoT Devices: Sustainable Eco-Friendly Manufacturing, Energy Harvesting, and Wireless Connectivity

HAMED RAHMANI [1] (Member, IEEE), DARSHAN SHETTY [2] (Student Member, IEEE),
MAHMOUD WAGIH [3] (Member, IEEE), YASAMAN GHASEMPOUR [4] (Member, IEEE),
VALENTINA PALAZZI [5] (Member, IEEE), NUNO B. CARVALHO [6,7] (Fellow, IEEE),
RICARDO CORREIA[6] (Member, IEEE), ALESSANDRA COSTANZO [8] (Fellow, IEEE),
DIEFF VITAL [9] (Member, IEEE), FEDERICO ALIMENTI [5] (Senior Member, IEEE), JEFF KETTLE [3],
DIEGO MASOTTI [8] (Senior Member, IEEE), PAOLO MEZZANOTTE [5] (Member, IEEE),
LUCA ROSELLI [5] (Fellow, IEEE), AND JASMIN GROSINGER [10] (Senior Member, IEEE)

(Invited Paper)

[1]IBM T. J. Watson Research Center, Yorktown Heights, NY 10598 USA
[2]Infineon Technologies Austria AG, 8020 Graz, Austria
[3]James Watt School of Engineering, University of Glasgow, G12 8QQ Glasgow, U.K.
[4]Department of Electrical and Computer Engineering, Princeton University, Princeton, NJ 08540 USA
[5]Department of Engineering, University of Perugia, 06125 Perugia, Italy
[6]Departamento de Eletrónica, Telecomunicações e Informática, Universidade de Aveiro, 3800 Aveiro, Portugal
[7]Instituto de Telecomunicações, 3800 Aveiro, Portugal
[8]DEI "Guglielmo Marconi", University of Bologna, 40126 Bologna, Italy
[9]Department of Electrical and Computer Engineering, University of Illinois Chicago, Chicago, IL 60607 USA
[10]Institute of Microwave and Photonic Engineering, Graz University of Technology, 8010 Graz, Austria

CORRESPONDING AUTHOR: Jasmin Grosinger (e-mail: jasmin.grosinger@tugraz.at).

ABSTRACT This invited paper presents potential solutions for tackling some of the main underlying challenges toward developing sustainable Internet-of-things (IoT) devices with a focus on eco-friendly manufacturing, sustainable powering, and wireless connectivity for next-generation IoT devices. The diverse applications of IoT systems, such as smart cities, wearable devices, self-driving cars, and industrial automation, are driving up the number of IoT systems at an unprecedented rate. In recent years, the rapidly-increasing number of IoT devices and the diverse application-specific system requirements have resulted in a paradigm shift in manufacturing processes, powering methods, and wireless connectivity solutions. The traditional cloud-centering IoT systems are moving toward distributed intelligence schemes that impose strict requirements on IoT devices, e.g., operating range, latency, and reliability. In this article, we provide an overview of hardware-related research trends and application use cases of emerging IoT systems and highlight the enabling technologies of next-generation IoT. We review eco-friendly manufacturing for next-generation IoT devices, present alternative biodegradable and eco-friendly options to replace existing materials, and discuss sustainable powering IoT devices by exploiting energy harvesting and wireless power transfer. Finally, we present (ultra-)low-power wireless connectivity solutions that meet the stringent energy efficiency and data rate requirements of future IoT systems that are compatible with a batteryless operation.

INDEX TERMS Antennas, backscattering, biodegradable, CMOS, energy harvesting, green substrates, harmonic transponders, MTT 70th Anniversary Special Issue, recyclable electronics, rectifier, RFID, system-on-chip, sustainable IoT, wireless power transmission.

I. INTRODUCTION

The evolution of "Internet-of-Things" has opened limitless potential solutions to enable the world around us to function more intelligently and efficiently. A widespread network of devices with sensing, processing, and communication capabilities is a powerful tool to revolutionize every aspect of our lives. An excellent testament to this statement is the emergence of IoT devices in various applications such as smart cities, intelligent agriculture, enhanced robotics, manufacturing, wearables, implants, and health monitoring systems. [1], [2], [3]. The use cases for some of these applications and their projected global economic value by 2035 are demonstrated in Fig. 1. These emerging applications impose strict performance requirements on IoT devices that a paradigm shift toward intelligent distributed systems could only address. The traditional cloud-centering schemes are expected to be replaced by distributed innovative configurations to meet future IoT technology's diverse system requirements, e.g., latency, power consumption, and reliability. The fast adoption of IoT technology in various applications has yielded an explosive number of IoT devices, and the number of connected objects is expected to surpass 43 billion by 2023 [1].

To ensure that IoT technology can sustainably grow to be a part of the future connected world, we need to consider the potential environmental, economic, and societal impacts and challenges – to name a few – introduced by the massive upscaling of IoT devices and address them in the early stages of IoT ecosystem development. For example, raw materials used for manufacturing, supplying energy to ubiquitous IoT devices, and getting rid of the eco-toxicity of batteries will be a prevalent part of this new IoT ecosystem. However, the emerging use cases impose demanding requirements, e.g., operating range, latency, and reliability. In some cases, the traditional design techniques and technologies are inadequate and cannot meet the required specifications. Thus, the sustainable growth of IoT devices could be enabled by: 1 – Addressing environmental concerns by using eco-friendly materials, reducing carbon footprints, and removing toxic materials from the manufacturing processes. 2 – Exploiting energy harvesting and wireless power transfer technologies to get rid of the eco-toxicity of batteries at the IoT device side or at least to reduce the cost of battery replacement. Furthermore, 3 – Enhancing or inventing new communication and sensing methods by applying (ultra-)low-power or batteryless communication technologies capable of meeting the stringent design requirements.

This article discusses eco-friendly manufacturing, sustainable powering, and wireless connectivity for next-generation IoT devices and presents unique design solutions for these challenges. In particular, the invited paper presents IoT design solutions from MTT-S's technical committee members of TC-26 RFID, Wireless Sensors, and IoT Committee. Section II reviews eco-friendly manufacturing for next-generation IoT devices, presenting alternative biodegradable and eco-friendly options to replace existing materials. Section III discusses sustainable powering IoT devices by exploiting energy harvesting and wireless power transfer. Section IV discusses low-power wireless connectivity solutions that meet stringent energy efficiency and data rate requirements of future IoT systems compatible with a batteryless operation. Section V concludes the work.

II. ECO-FRIENDLY MANUFACTURING OF IoT DEVICES

The environmental footprint of pervasive IoT devices, including flexible and large-area electronics, must be factored into the early design stages of IoT networks. In this section, we focus on the sustainability issues of current manufacturing processes and highlight the new opportunities and research trends on wireless devices implemented on green substrates.

A. SUSTAINABLE MANUFACTURING AND RECYCLING

IoT products based on conventional electronics could suffer from similar sustainability issues, and unintended outcomes will afflict consumer electronics [4], [5], including:

- Heavy reliance on Critical Rare Metals (CRMs) used in most electronics components (e.g., batteries, energy harvesters, integrated circuits), some of which are depleting and almost 100% dependent on imports.
- Emissions from the manufacturing process; the electronics sector is identified as one of the top 8 sectors that account for more than 50% of global carbon emissions, with 77% coming from the supply chain [6].
- At the End-of-Life (EoL), IoT devices are classified as Waste Electrical and Electronic Equipment (WEEE) by the EU's Directive (2012/19/EU). The WEEE is a particularly pertinent problem and is the fastest growing waste stream globally; approximately 50 million tonnes of WEEE is produced, growing at 3–5% per year. Less than 20% of generated WEEE is formally recycled internationally. Rapidly expanding global demand for IoT products makes the current 'take-make-waste' model of consumption unsustainable [7].

There is no mainstream circular economy approach for electronics and, thus, IoT products. Encouraging the repair and reuse of IoT products is the best method to encourage circular electronics and to improve the sustainability [8], but this may not be enough in the short term as the use of IoT devices rises. Fig. 2 highlights two *complementary* approaches to manufacturing sustainable devices: (a)–(c) robust, recyclable, and re-usable devices; and (d)–(g) bio-derived and biodegradable electronics [9], potentially leading to zero-waste IoT but often possessing lower performance.

Improving the durability of flexible and harsh-environments electronics is essential for sustainability improvement. Structural integrity can be preserved using vacuum-formed organic polymer encapsulation of discrete components, e.g., passives, RF and analog Integrated Circuits (ICs), and antennas [10], to withstand cyclic bending and washing. As in Fig. 2(a), such encapsulation is conformable

$13.2 Trillion in global economic value by 2035

Precision agriculture
$389B

Construction and mining
$1,061B

Digitized education
$258B

Connected healthcare
$1,056B

Reacher mobile experiences
$2,291B

Smart manufacturing
$4,687B

Intelligent retail
$1,198B

Smart city
$2,242B

FIGURE 1. Expansion of the mobile ecosystem to future applications of IoT devices and the projected global economy value by 2035 [1].
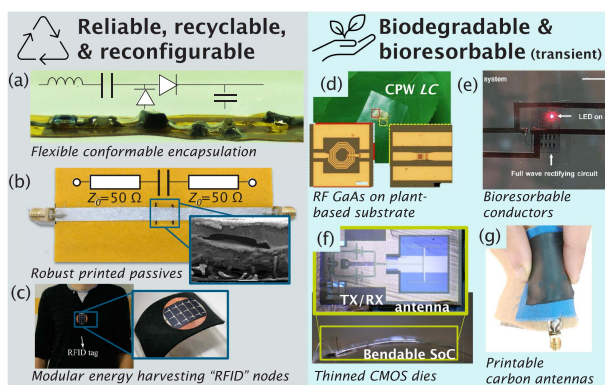

FIGURE 2. From reusable to disposable sustainable devices: (a) robust encapsulation of flexible RF circuits [14]; (b) mechanically and thermally-reliable passives replacing discrete parts [12]; (c) programmable and modular flexible sensing platforms [15]; (d) cellulose nanofibril-based RF passives [16]; (e) bioresorbable Mg antennas and diodes [17]; (f) ultra-thin bendable RFIC [18]; (g) biodegradable carbon antennas [19].

and does not significantly add to the thickness or weight of a flexible circuit. Both the flexibility and power handling can also be improved by replacing ceramic discrete components with printable passives [11], [12], as demonstrated in a 50 GHz DC-blocking line using screen-printed capacitors, seen in Fig. 2(b) [12].

Modular and re-configurable hardware is crucial in increasing the lifespan of IoT nodes. For instance, the approach of using a single device, a wearable antenna in Fig. 2(c), as a platform for mounting multiple sensors and energy harvesters (flexible solar cells) can be re-configured during the device lifetime by adding new sensing interfaces. Moreover, designers could extend the antenna's role to act as a simultaneous wireless power receiver [13], reducing the number of required components while adding functionality.

Several biodegradable materials and components have been proposed while moving to transient and disposable devices. Wood-based cellulose nanofibril (CNF) substrates have been used for RF passives and low-density digital logic circuits [16]. GaAs diodes were also packaged in CNF, demonstrating green RF energy harvesters [16]. Biodegradable and bio-compatible, i.e., bioresorbable, devices leveraging magnesium (Mg) find applications in wireless biomedical sensing, where an all Mg-based rectennas was previously demonstrated [17]. Antennas have also been realized using poly(3,4-ethylenedioxythiophene) polystyrene sulfonate (PEDOT:PSS) [20], [21] and carbon black [19], both of which are biodegradable conductors [5]. A broadband PEDOT:PSS antenna was characterized up to 20 GHz showing a radiation efficiency exceeding 80% [21]. Printing a PEDOT:PSS antenna on textiles for off-body communication resulted in a radiation efficiency of around 28% [20]. Fig. 2(g) shows a carbon black S-band microstrip antenna printed directly on textiles for wearable applications. The approach of printing biodegradable conductive tracks on degradable substrates is key to minimizing the PCB disposal waste arising from commercial-grade FR4 substrates, adhesives, and the waste generated during the photolithography process.

Nevertheless, we can only realize devices such as high-density logic circuits or millimeter wave (mmWave) frontends in complementary metal-oxide semiconductor (CMOS) or monolithic microwave integrated circuit (MMIC) processes. Therefore, rigid semiconductor die thinning is a common approach for realizing bendable and potentially biodegradable ICs, while retaining most of the performance of conventional ICs. Recently, a 120 GHz transmitter with an on-chip antenna was fabricated in a standard SiGe BiCMOS process and demonstrated high mechanical flexibility after being thinned to 20 μm [18]. The reduction in the die's thickness resulted

in around 4 dB loss in the radiated power output but had a minimal influence on the frequency stability. Fig. 2(g) shows the bendable RFIC.

While biodegradable electronics offer exciting possibilities to eliminate WEEE, most commercial and research efforts of EoL have focused on minimizing WEEE by recycling. Recycling of WEEE generally follows a sequential approach; removable or bulky components are manually dismantled. Afterward, the particle sizes are progressively reduced by shredding, crushing, pulverizing, grinding, and (sometimes) ball milling. After the pulverization step, different separators are used to separate raw metal and non-metal materials [5]. This might create a particular challenge for sensing devices attached to, e.g., food packaging. Such products would have to be treated as WEEE rather than standard plastic waste.

The obsolesce of IoT devices is resulting in large electronic waste. Consumers must take back their broken devices to the original manufacturer for repairs. However, there have been rising movements to remove monopolistic repair tactics and restore the right of repair to consumers. These movements seek repair-friendly policies and regulations to enable consumers and third parties to repair and modify electronic devices. Hence, it will empower consumers to behave more sustainably by reducing the WEEE, directly and indirectly, [22]. For example, the EU introduced new rules in 2021, with similar initiatives already in force in the USA. These challenges are not insurmountable but need deeper considerations as researchers develop other products.

B. GREEN MATERIALS

Recurring low-environmental-impact materials and processes are essential to prevent future risks of electronics pollution (e-pollution) and to foster a granular distribution of autonomous wireless devices. Substrates are most of the mass of electronic printed circuit boards (PCBs). Therefore, replacing standard highly polluting substrates (such as FR4 epoxy glass laminates) with green materials helps to significantly reduce the volume of toxic electronic waste (e-waste).

Green Materials include both recyclable (i.e., materials that can still be reused at the EoL stage of electronics) and biodegradable materials (i.e., materials that can be decomposed by living organisms and do not pose any environmental risks). The most popular green materials are paper and bio-plastics, such as polylactic acid (PLA). The electromagnetic properties of common green substrates used for electronics are shown in Table 1. They have unique mechanical and optical properties, allowing innovative sensing solutions. However, these materials are not specifically made for electronics and radio-frequency components and can feature variable electromagnetic properties and high dielectric loss. Additionally, they cannot withstand high temperatures (for instance, the glass transition temperature of PLA is about 60 °C [23]), which limits the processes and materials that we can use to manufacture the circuits. Hence, research trends on eco-friendly implementation of IoT devices focus on addressing the shortcomings of the green substrates by innovative design

TABLE 1. Electromagnetic Properties of Common Green Materials

Ref.	Material	Freq. (GHz)	ϵ_r	$\tan\delta$
[24], [25]	paper	0-10	2.55	0.05
		24	2.52	0.04
[26]	cork	0.75-0.95	1.49-1.91	0.18-0.45
[23], [27]	PLA	0.72	2.8	0.008
		10	2.575	0.016
		40	2.536	0.019
		60	2.517	0.020
[28]	PHBV*	7.35	2.83	0.006
		21.8	2.9	0.009
		35.55	2.65	0.015

*poly(3-hydroxybutyrate-co-3-hydroxyvalerate)

(a)

(b)

(c)
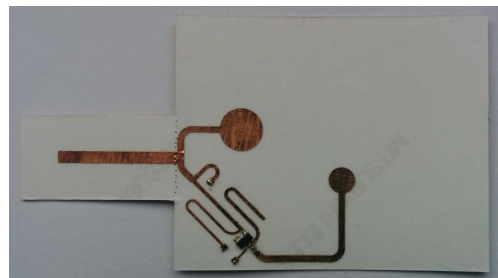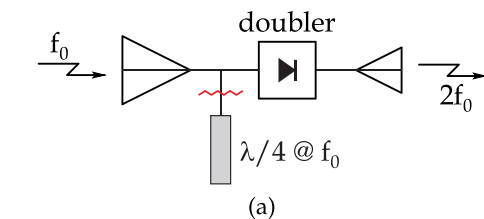
FIGURE 3. Harmonic crack sensor: (a) schematic, (b) photo of the intact sensor, and (c) photo of the cracked sensor. From [29].

and taking advantage of their unique properties to enable novel low-power sensing and telemetry schemes. Here a few examples of RF circuits and sensors based on paper and PLA are reported, where green materials are used not only as dielectric substrates but also as sensors.

Fig. 3 shows a wireless passive harmonic crack sensor manufactured on a paper substrate. The transponder is based on harmonic backscattering: the tag is interrogated with a

**TABLE 2.** Comparison With State-of-the-Art Passive Crack Sensors

Ref.	Transponder type	Sensing strategy	Substrate	Freq. (GHz)	Pt EIRP (dBm)	Max tag-to-reader distance (m)
This work	Harmonic	Stub removal	Paper	2.45;4.9	25	5
[30]	Chipless	Resonator frequency shift	Taconic CER-10-0500	2-6	0*	0.3
[31]	Chipless	Resonator frequency shift	Rogers RT/Duroid 6010.2LM	2-8	/	0.06533
[32]	Harmonic	Resonator frequency shift	Rogers RT/duroid 5880	2.78-2.89;5.56-5.78	15	0.5
[33]	UHF RFID	RSSI	No substrate	0.915	36	0.75
[34]	Chipless	Time domain reflectometry	Taconic TLX-0	2-20	/	0.3
[35]	UHF RFID	Phase difference	FR4	0.867	/	0.9
[36]	UHF RFID	Resonant frequency shift	FR4	0.90275-0.92725	36	1

* the antenna gain of the transmitter is not reported

sinusoidal signal with frequency f_0 and responds at the second harmonic. The sensor consists of an open-circuited stub placed in a shunt with the input port of a passive frequency doubler. Two antennas, working at harmonic frequencies, complete the circuit. The stub is a quarter-wave long at f_0. Therefore, the input signal is short-circuited when the tag is intact, and no second harmonic is generated. On the other hand, when the stub is torn off, the input signal reaches the frequency doubler, and a second harmonic signal is generated and backscattered. The reader detects this signal which plays the role of an alarm. It is worth noting that, unlike traditional radio backscattering, no coding is needed to separate the tag response from the clutter reflections, allowing for a fully passive, simple, and long-range transponder. The metal traces are manufactured by applying photo-lithography to an adhesive copper laminate (alternatively, laser cutting can be used) which is finally stuck to the substrate. Two lumped components (a ceramic capacitor and a Schottky diode) are soldered to the metal traces. In the reported study, with $f_0 = 2.45$ GHz, the authors observed a transmitted power of 25 dBm effective isotropic radiated power (EIRP) and a receiver sensitivity of -100 dBm, an operating range from 1 to 5 m. In this example, the fragility of the paper is leveraged to manufacture a disposable crack sensor. At the same time, a simple yet effective tag architecture allows us to minimize the number of surface-mount commercial components.

Table 2 compares the proposed crack sensing system with other passive wireless crack sensors at the state of the art. As can be seen, the proposed solution outperforms other passive crack sensing solutions for its read range, and it represents a competitive alternative green solution compared to the other circuits manufactured on standard PCBs.

In [37], the porosity of paper is used to realize a humidity sensor instead. The transducer is based on a series resonator, with a variable capacitance consisting of a paper-aluminum bimorph cantilever above a rigid metal plate. As the relative humidity increases, the length of the paper layer increases to that of the Al layer, thus determining the cantilever deflection.
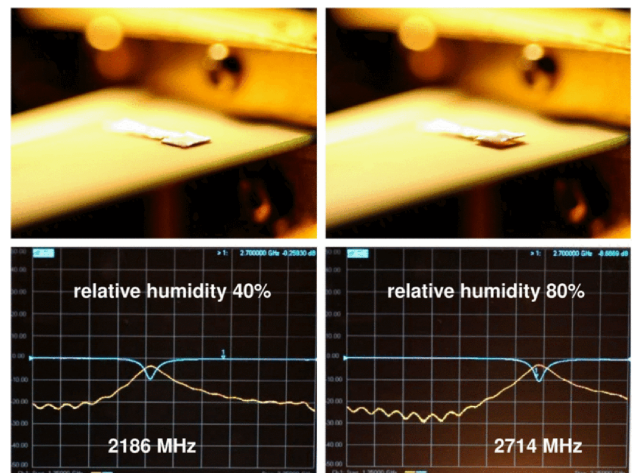
FIGURE 4. Bimorph paper-aluminum cantilever photographs and measured scattering parameters for two values of relative humidity (RH), 40% RH (left panels) and 80% RH (right panels): As the relative humidity increases, the cantilever bends, reducing the filter capacitance. Consequently, the reflection coefficient peak (yellow line) moves from 2186 MHz to 2714 MHz. From [37].

The consequent capacitance decrease causes a frequency shift of the filter notch frequency, as shown in Fig. 4. This sensor can be read wirelessly by simply connecting the resonator to an antenna, leading to a chipless tag.

The same hybrid approach adopted for the harmonic crack sensor, involving an alternative flexible substrate, copper adhesive laminate, and discrete lumped components, is used to manufacture an autonomous radio-frequency identification (RFID) sensor for precision agriculture [23]. The sensor is based on a commercial RFID chip (model EM4325 from EM Microelectronic) with an integrated temperature sensor; the chip is connected to a folded dipole antenna manufactured on a PLA substrate. The chip can operate in passive mode and semi-active mode. In the passive case, the interrogating RF signal transmitted by the reader is used both for backscatter communication and to activate the transponder circuitry. In
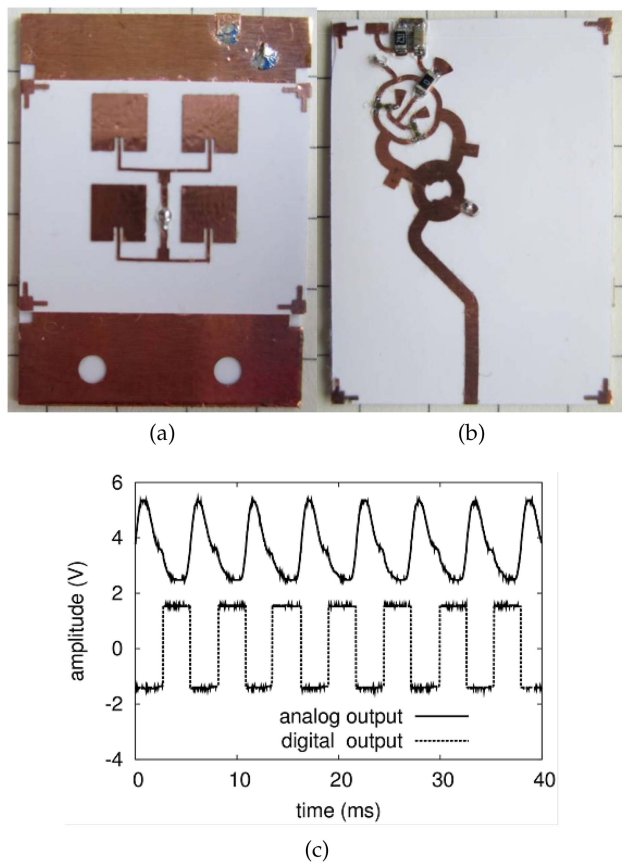
FIGURE 5. 24-GHz Doppler radar front-end on cellulose: (a) Layout of the top layer. (b) Layout of the bottom layer. (c) Output signal obtained by observing the movement of a cooling fan at a 1 m distance from the radar. The circuit area is 35 mm x 28 mm. After [39], [40].

a semi-active case, the interrogation signal is used only for communication, while an additional energy source is used for the circuitry, which increases the chip sensitivity significantly. In the proposed solution, flexible solar cells from Ribes Tech provide the extra power the tag needs in semi-active mode. Leveraging the transparency of the PLA substrate, future developments can be envisioned in which the same transparent substrate is used both for the antenna and for the solar cell [38].

In [39], [40], for the first time, a 24-GHz radar front-end and its antenna were integrated on a multilayer cellulose-based substrate, manufactured by alternating paper, glue, and copper layers. The circuit exploits a distributed microstrip structure that is realized using a copper adhesive laminate, which guarantees a low conductive loss. The radar shown in Fig. 5 operates at 24 GHz and transmits 5 mW of power. The antenna has a gain of 7.4 dBi and features a half-power beam width of 48 degrees. The sensor has a size of a stamp. It can detect the movement of a walking person up to 10 m in the distance, measuring a minimum speed of 5 cm/s up to 3 m/s. This experiment demonstrates that circuits on cellulose can operate at record frequencies and that ultra-low cost, green (i.e., recyclable and biodegradable) materials can be a viable

solution to implement, at least in part, the radio-frequency hardware for the upcoming IoT era.

In all of the above-described solutions, the transponders feature some residual non-recyclable parts due to a few commercial lumped components and interconnects that must be separately discarded. Significant research is being done on realizing green organic non-linear devices. So far, the limiting factor is represented by the reduced transit frequency of the developed diodes and transistors. In [48], an attempt to obtain a close to 100% green harmonic transponder (tag) is reported. The harmonic tag is based on a pentacene diode, and a couple of concentric copper coils stuck on a paper substrate. The tag, operating at 7.5 MHz, although still characterized by a short read range and high conversion loss, represents a promising way for future all-natural IoT electronics.

The proposed solution on paper is compared with other 24 GHz state-of-the-art radar frontends in Table 3. Although we currently find integrated radar frontends up to sub-THz frequencies, this work demonstrates the possibility of implementing multilayer RF frontends on paper at millimeter waves.
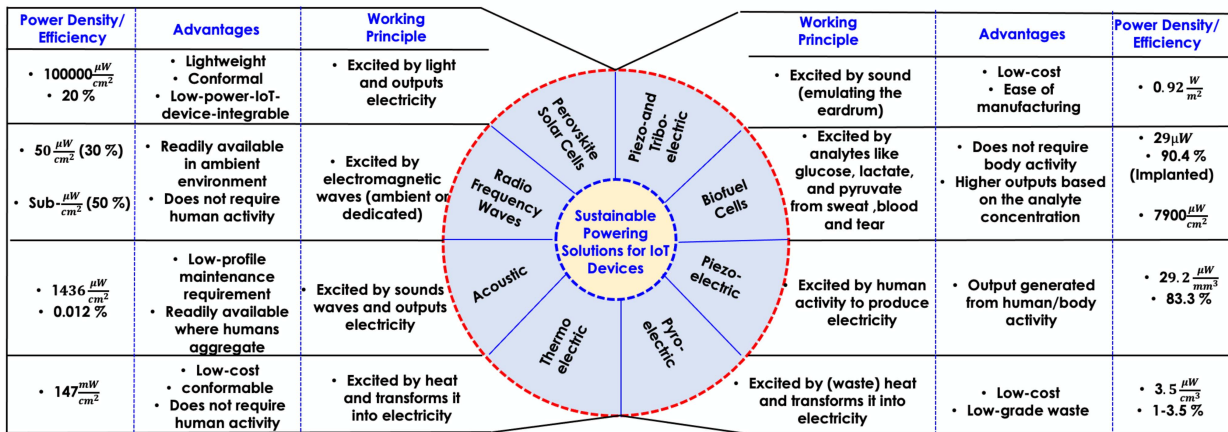
III. SUSTAINABLE POWERING IoT DEVICES
The urge for energy-independent electronic devices is intensifying with the advances in IoT technology. Currently, the most common solution for powering electronics is batteries. On the other hand, recent advances in semiconductor technology have resulted in a significant integration capability and size reduction of electronics. Yet, the overall size of an IoT device is not scaled at the same rate since it is dominated by the size of powering and energy storage components. State-of-the-art batteries have centimeter-scale footprints due to the limited power density of energy storage technologies. They fail to address the demands of long-term miniaturized devices. In addition, the raw materials used in battery manufacturing, such as lead, fluorinated electrolytes, and cobalt, are toxic and lead to undesired consequences. Therefore, it is essential to eliminate batteries from IoT devices and explore alternative powering sources for realizing self-powered devices.

A. ENERGY HARVESTING
In the past few years, various energy harvesting techniques have been proposed to tackle the issues of battery-powered devices. Some major advantages of using energy harvesting are: 1 – They are easy to manufacture and reduce the cost and rounds of maintenance. 2 – They result in much less carbon emission compared with battery-based solutions. 3 – They can be implemented on green materials (substrates) that are biodegradable [71], bio-compatible, pollution-free [61]. 4 – They are easily integrated with readily available wireless communication systems [71]. The energy sources can be categorized as ambient and dedicated energy sources. The ambient energy sources are more attractive because they do not require any additional power transmission link and utilize already-existing energy sources, solar, wind, motion, and RF radiations. However, in many wireless applications, ambient

TABLE 3. Comparison With 24 GHz State-of-the-Art Doppler Radar Frontends

| Ref.	Technology	Antenna gain (dBi)	Ptx (dBm)	Range (m)	Vmin (mm/s)	Size (mm^2)
This work	Cellulose multi-layer	7.4	7	10	50	20 x 27
[41]	RO3003 and FR4	7	15	2	0.5	90 x 65
[42]	LTCC and FR4	n.a.	n.a.	n.a.	0.8	30 x 30
[43]	LTCC	n.a.	20*	70	n.a.	34 x 21
[44]	LTCC	8.6	15*	30	n.a.	25 x 25
[45]	Discrete comp.	18	6	300	n.a.	79 x 79
[46]	Cellulose single layer	7	3	n.a.	n.a.	35 x 28
[47]	SiGe (Sense2Gol. demo)	10	4	15	139	25 x 25

FIGURE 6. Summary of different sustainable powering solutions for IoT devices with parameters including types of system (energy source), working principle, advantages, power density, and efficiency [49], [50], [51], [52], [53], [54], [55], [56], [57], [58], [59], [60], [61], [62], [63], [64], [65], [66], [67], [68], [69], [70].

energy sources do not guarantee the Quality-of-Service (QoS) due to uncertainties in time, location, and weather conditions. Dedicated energy sources, e.g., narrow beam RF radiations, are alternative energy sources to ensure reliability and QoS in wireless applications at the expense of higher cost and resources [72].

Fig. 6 reports a summary of some of the popular sources in energy harvesting applications along with their working principles, advantages, power density, and efficiency. The state-of-the-art sustainable energy sources include biofuel cells [73], enhanced tribo-electric/piezo-tribo-electric nanogenerators [61], [63], [74], perovskite solar cells [53], [75], acoustic energy sources [51], piezoelectric sources [60], thermoelectric generators [55], and pyroelectric energy sources [51], [59] with sensitivities of 7900 μW/cm^2, 2.5 W/m^2, 100000 μW/cm^2, 1436 μW/cm^2, 29.2 μW/mm^3, 147 mW/cm^2, 3.5 μW/cm^3 [51], respectively. Electromagnetic-based power transmission, in particular, is one of the most commonly used mechanisms in WPT and energy harvesting schemes [76]. Inductive coupling, ambient RF radiation, and dedicated RF radiations are three different types of EM-based energy harvesting schemes that enable various applications and provide a wide range of power densities. One of the most popular energy harvesting solutions is electromagnetic waves. However, we can use the RF energy

sources in ambient and dedicated fashions. Inductive WPT is commonly used in medical implants, wearables, and portable devices with a short operating range ($\leq$ 1 m). It is considered a dedicated energy source that is predictable, controllable, and achieves high efficiencies ($\geq$ 80%). The ambient RF radiation is commonly used for wireless sensor nodes with an operating range of a few tens of meter and provide a power density of 0.2 nW/cm^2~1 μW/cm^2. On the other hand, RF radiation can be used as a dedicated energy source to guarantee reliability and contractility. A dedicated RF radiation requires additional resources to ensure energy transmission is carried through a dedicated link and can function at long operating ranges (hundreds of meters) by focusing the radiated beam and operating at GHz or mmWave frequency ranges [72].

Hybrid energy harvesters have been considered to improve the reliability of battery-free IoT devices. Multiple energy sources are combined to alleviate the limitations of a particular energy source. For instance, solar cells cannot operate at night, but ambient or dedicated RF radiation can be used in the absence of light [77]. EM-based techniques are emerging among various energy sources as promising generic solutions compatible with next-generation IoT devices. EM radiation at a higher frequency range makes it possible to integrate energy harvesting circuitry and components on commercial CMOS
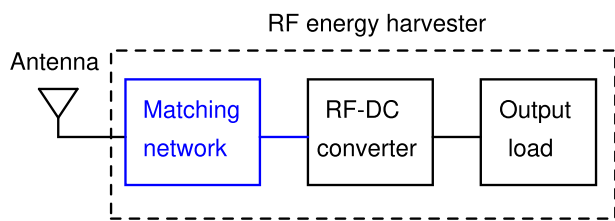
FIGURE 7. Conceptual schematic of an RF energy harvester with an optional matching network.

FIGURE 8. RF energy harvester prototypes on Rogers 4350B boards: (a) design-I with a matching network to interface to a 50 Ω antenna and (b) design-II with a matched single-ended loop antenna.

technology to realize low-cost and miniaturized system-on-chip (SoC) IoT devices [78], [79], [80].

B. RF ENERGY HARVESTERS

The ambient RF radiation with a power density of several nW/cm^2 opens up applications of sustainable batteryless wireless sensor nodes with minimal functional capabilities. These batteryless wireless sensor nodes can be deployed in harsh and remote environments for sensing and monitoring applications [81]. The batteryless operation improves the sustainability of the sensor nodes, ensuring zero battery replacement and low maintenance costs. The batteryless wireless sensor nodes are driven by an RF energy harvester which harvests the incoming RF energy to DC energy. Given the low available input RF power, the performance of the RF energy harvester depends on the PCE, the startup sensitivity, and the strength of the incident RF energy [82].

Fig. 7 shows the conceptual picture of an RF energy harvester. The RF energy harvester typically includes an antenna, an optional matching network, an ultra-low-power (on-chip) RF-DC converter, and an output load. The ultra-low-power RF-DC converters in [83], [86], [87], [88], [89], [90], [91], [92], [93], [94] have a very high input impedance that is of capacitive nature. It presents a challenge to match the RF-DC converter to a 50 Ω system.

Here, we delve into the challenges and possible solutions for designing RF energy harvesters for the target batteryless wireless sensor nodes. We present two specific implementations of RF energy harvesters optimized for high-power conversion efficiency and ultra-low-power startup. The presented RF energy harvesters include the ultra-low-power RF-DC converter in [83]. However, the presented RF energy harvesters can also be designed using the ultra-low-power RF-DC converters in [86], [87], [88] and [93]-[94]. The RF-DC converter sub-system designed in an Infineon 130 nm CMOS process is a modified Dickson charge pump with threshold compensated CMOS diodes, which help to achieve a low-power startup.

Design-I of the RF energy harvester shown in Fig. 8(a) includes the RF-DC converter mounted on a low-dielectric Rogers 4350B board, including an L-matching network. In post-layout simulations, the RF-DC converter shows an input impedance of 2-j240 Ω at 868 MHz. The ultra-low-power nature of the RF-DC converter demands an L-matching network comprising a high-quality (Q) factor 27 nH CoilCraft^{TM} RF
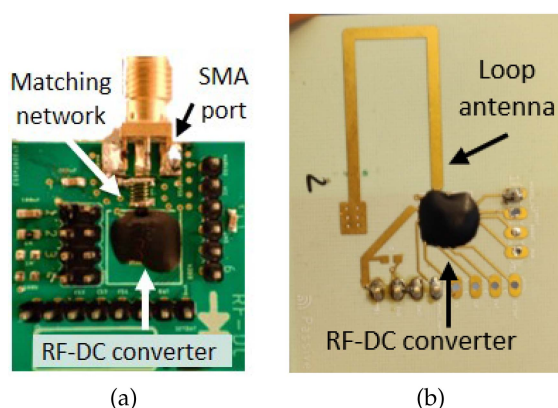
inductor and a 10 pF ATC RF capacitor to connect to a 50 Ω antenna.

The design-II includes a conjugate-matched single-ended loop antenna directly connected to the RF-DC converter to achieve resonance at 868 MHz. The single-ended loop antenna on a Rogers 4350B substrate in Fig. 8(b) is designed using electromagnetic (EM) simulations with an impedance of (2+j240) Ω to power-match the chip impedance and a maximum realized gain of 1 dBi [84]. The RF-DC converter has been optimized for sub-microwatt input power startup. Thus, the single-ended loop antenna has been designed to match the RF-DC converter's input impedance at this power level of −30 dBm.
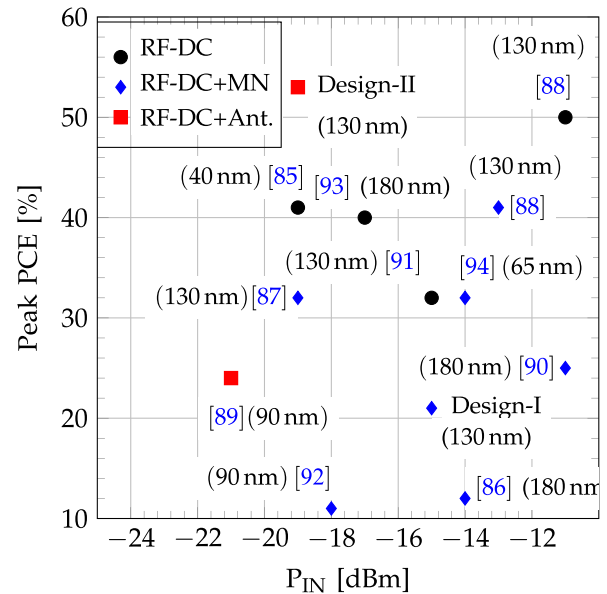
The measurement results of the two designs of the RF energy harvester at 868 MHz are shown in Fig. 9, i.e., the sensitivity and PCE. For a fair comparison, the antenna gain of design-II has been de-embedded to compare the performance of the two RF energy harvester designs. Design-I, which includes a matching network, suffers from an additional insertion loss due to the limited quality factor of the lumped components. In comparison, design-II consists of a matched single-ended loop antenna and avoids lumped elements in the design. As a result, as shown in Fig. 9(a), the RF energy harvester achieves a 1 V sensitivity of −20 dBm for design-I and −25 dBm for design-II. At a higher power level of −10 dBm, most of the input power is delivered to the RF-DC converter. As a result, the insertion loss of the matching network is less significant; here, the performances of design-I and design-II are comparable. The PCE versus input power P_{IN} curves in Fig. 9(b) highlight a much better design-II efficiency than design-I for a load of 1 M Ω at 868 MHz. Design-I achieves a peak PCE of 53% at −17 dBm (20 μW), which implies that roughly 10 μW is harvested at the output. At lower input power levels of 4 μW, 1 μW is gathered at the output by design-I. This harvested power is sufficient to power up an ultra-low-power wake-up receiver [95], temperature sensor [96], and power management circuits [97], [98] of an IoT device.
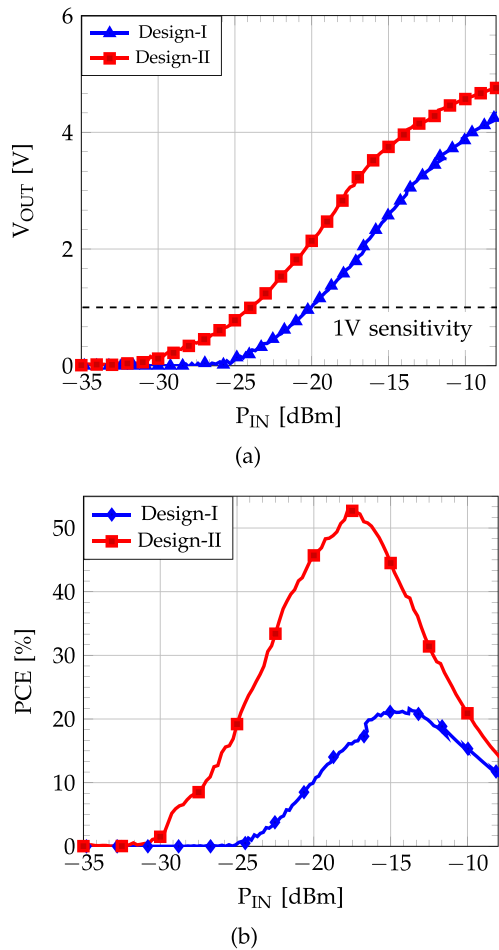
FIGURE 9. Performance of the RF energy harvesters for a 1 MΩ output load: (a) output voltage V_{OUT} versus input power P_{IN} and (b) power conversion efficiency versus P_{IN} (f = 868 MHz).

FIGURE 10. Performance overview of the peak PCE of the various ultra-low-power sub-1 GHz RF energy harvesters including their technology nodes (R_L=1 MΩ). The listed works can be classified into three categories: RF-DC converter, RF-DC converter and the matching network, and RF-DC converter and a matched antenna.

Two-port Network
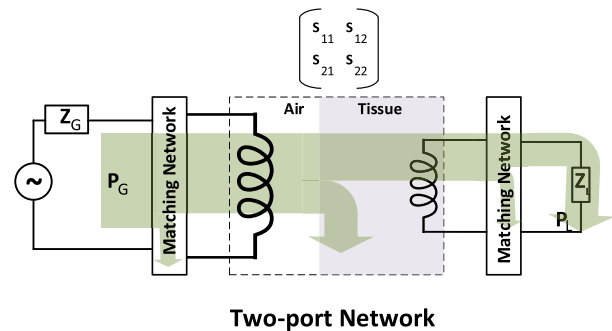
FIGURE 11. Power flow in the wireless link of a WPT system for medical implants [101].

In comparison, state-of-the-art ultra-low-power RF energy harvesters have been reviewed and listed in Fig. 10. The RF energy harvesters have all been designed for sub-1 GHz frequency industrial, scientific, and medical (ISM) bands. The RF energy harvesters shown in Fig. 10 can be classified into three categories: RF-DC converter, RF-DC converter with a Matching Network (MN), and RF-DC converter with a matched antenna (Ant.). The works in [85], [88], [91], and [93] present low-power startup RF-DC converters where the losses of the matching network have been de-embedded. As a result, the RF-DC converters have a high peak PCE between 30%–40%. The inclusion of the matching network losses has a strong impact on the peak PCE due to the high insertion losses as seen in Design-I, [86], [88], [90], [92], and [94]. Including a power-matched antenna to avoid a matching network greatly benefits the ultra-low-power RF energy harvesters, as shown in Design-II and [89]. Despite a low PCE, the work in [90] achieves a good PCE at a low power level of −21 dBm. Fig. 10 also highlights an interesting trend in RF energy harvesters which are predominantly designed in the older CMOS technology nodes like 90 nm, 130 nm,

and 180 nm. The older technology nodes offer metal oxide semiconductor transistors with much lower leakage, which is highly beneficial for the design of RF energy harvesters.

The results show that for an ultra-low-power design and batteryless sensor nodes, power-matching of the antenna becomes more and more critical compared to Ultra-High Frequency (UHF) RFID tags [99], [100]. It is highly advantageous to design an RF energy harvester that includes a conjugate-matched loop antenna for ultra-low-power harvester applications.

C. WIRELESS POWER TRANSFER

Modeling an EM-based WPT system using a two-port network is a generic approach for modeling a WPT system since we can apply it to both near-field and far-field EM operating regions [101]. Fig. 11 shows a conceptual inductive WPT scheme where the wireless link is composed of air and biological tissues. The overall power transfer efficiency (PTE) is

defined as the delivered power to load of the power harvesting system P_{load} over available power by the generator P_G.

The PTE can be viewed as a multiplication of wireless link efficiency η_{link} and RF to DC conversion efficiency η_{RF-DC}. The power receiving coil/antenna is one of the critical components in a wireless power receiver and creates a dilemma in choosing the operating frequency. It is desired to operate the system at a higher frequency to utilize millimeter-sized antennas/coils with acceptable efficiencies. On the other hand, the propagation path loss is a function of frequency. The link efficiency can be defined as the ratio of the delivered power to the load of the two-port network over the generated power by the RF source. It can be divided into three distinguished terms (see Fig. 11):

$$\eta_{link} = \frac{P_L}{P_G} = \eta_{m,Tx} \times \eta_{2port} \times \eta_{m,Rx}. \quad (1)$$

The η_{2port} term contains power losses in the coils and the intervening medium. In contrast, the $\eta_{m,Tx}$ and the $\eta_{m,Rx}$ represent the power losses due to impedance mismatch at the TX and RX sides, respectively. The received RF signal should be converted into a stable DC voltage to power the embedded electronics. The RF to DC conversion is usually done by a voltage rectifier and regulator. Therefore, η_{RF-DC} can be considered as multiplication of rectifier efficiency η_{rec} and regulator efficiency η_{reg}. While the operating frequency is usually determined by the standards, in some applications, such as medical implants, it can be chosen to optimize the performance of the link. However, the operating frequency is not the only controlling factor in the overall PTE. For instance, voltage rectifiers are known to be non-linear components, and their conversion efficiency is a string function of the input power and loading, as shown in the following expression:

$$\eta_{rec}(P_{in}, R_L, f) = \frac{P_{DC}}{P_{in}}. \quad (2)$$

For a given transmitted power, the received power may vary considerably, depending on the link composition, the orientation of the transmitter (TX) and the receiver (RX) antennas, and the load of the rectifier. Therefore, operating frequency and the matching network should be tuned adaptively to guarantee maximum PTE [102], [103], [104]. Moreover, the transmitted power level cannot be increased to compensate for the additional losses in the link as safety standards and regulations limit it. Specific absorption rate (SAR) is a perfect example of these regulations that limits human body exposure to EM waves [105], [106]. As a result of the link ambiguity and the limits of the transmission level, the maximum deliverable power to a millimeter-sized integrated power harvesting system is bound to ~100 μW, and ~ μW for near-field and far-field systems, respectively [78], [92], [101]. The power flow into a millimeter-sized fully-integrated IoT device is insufficient to continuously drive the power-hungry building blocks, e.g., wireless communication and stimulators. The remedy to this issue is duty-cycling the power-demanding building blocks operation to reduce the system's average
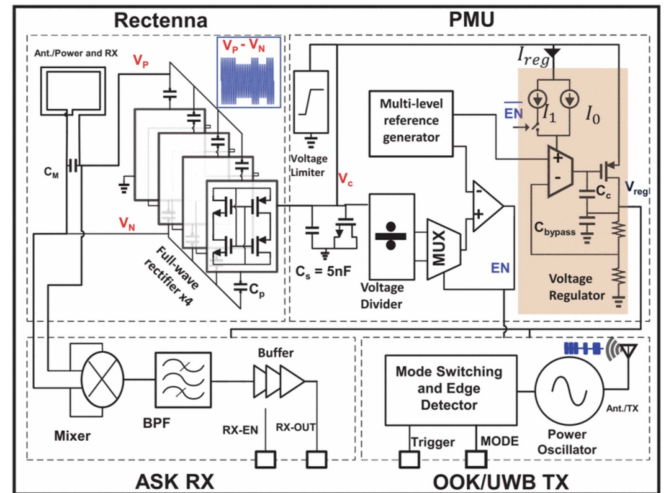
FIGURE 12. Block diagram of a fully integrated millimeter-sized data transceiver with a wireless power receiver and PMU [107].
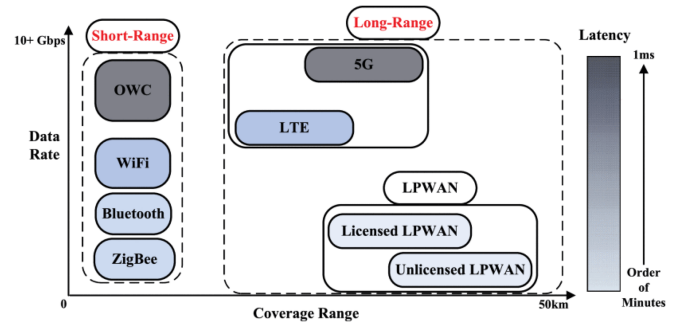
FIGURE 13. Illustration of IoT connectivity technologies' features in data rate, coverage, and latency [108].

power consumption. Fig. 12 shows an example of a fully integrated power harvesting system with a power management unit (PMU) to set the activation time of the data transmitter. Depending on the available RF power at the RX and the power consumption of the load, the PMU sets the power delivery state to continuous or duty-cycled mode, which enables the system to drive IoT devices with a wide range of power consumption.

IV. WIRELESS CONNECTIVITY FOR IOT DEVICES

Wireless connectivity is the core of IoT technology, enabling large-scale digitization by driving a paradigm shift from point-to-point monitoring to an all-connected-through-Internet scheme. Various IoT applications can be segmented into three major verticals: consumer (e.g., smart homes and wearables), enterprise (e.g., supply chain, asset tracking, and fleet management), and industrial (e.g., smart manufacturing, smart utilities, and robotic automation). Due to these applications' diverse and multifaceted nature, it is impossible to develop a unique wireless connectivity solution that fits all of these applications. The existing wireless connectivity technologies offer different operating ranges, data rates,

and latency, as shown in Fig. 13 [108]. The existing technologies have a natural trade-off between latency and power consumption. For instance, ZigBee and Bluetooth standards offer low-power consumption in short-range technologies, while Optical Wireless Communication (OWC) provides low latency. The same trade-off is observed in the long-range category between cellular (LTE/5G) and Low Power Wide Area networks (LPWANs).

Although the existing technologies have successfully addressed the needs of many applications so far, the mass scaling of IoT devices in future applications imposes more demanding specs on the maximum data rate, latency, and power consumption. Active research trends on low-power communication have been focused on improving the energy efficiency of the current ultra-low-power techniques, such as backscattering. Cellular wireless technology, 5G and beyond, has been a critical enabler of many modern IoT applications. It is envisioned we will accelerate the progress of wireless connectivity through the increased network agility, capacity to use secure devices, and integrated Artificial Intelligence (AI) offered by wireless technologies beyond 5G. Moreover, 5G and 6G wireless technologies operate at mmWave and sub-THz frequency ranges. Wireless connectivity could be expanded as a sensing tool, and new joint communication and sensing opportunities are offered.

The emerging applications of IoT systems instate high energy efficiency (required energy for successful wireless transmission per bit) and high data throughput on communication systems. Moreover, wireless connectivity solutions should support a high-density user population. In this section, we have focused on backscattering as one of the most energy-efficient modulation schemes, [109], and have provided the latest efforts on increasing the data rate of backscattering radios by 1 – using higher order modulation and 2 – increasing the operating frequency to millimeter waves and sub-THz region. In addition, we review an ultra-wide-band communication technique as one of the strong candidates for enabling low-power localization in a user-dense network.

A. QAM BACKSCATTERING

Traditional RFID systems and passive sensors use amplitude shift keying (ASK) and phase shift keying (PSK) for communication modulation. UHF RFID systems are a solution for substituting barcodes, having an increased interest in several approaches, such as non-line-of-sight communications and tracking. They are much more robust in harsh environments.

As presented before in [117], recent work [111] shows that higher-order modulation schemes can be used in RFID approaches also, this includes, for instance, 4-quadrature amplitude modulation (4-QAM). These modulation schemes increase the data rate by transmitting 2 bits as a single symbol, and thus in the long-range will reduce power consumption and increase read range. In [111], [118] a 4-QAM backscatter modulation is presented using a semi-passive system, in that case, a 3 V coin cell battery is used to power up the microcontroller. This microcontroller commands a quadrature phase
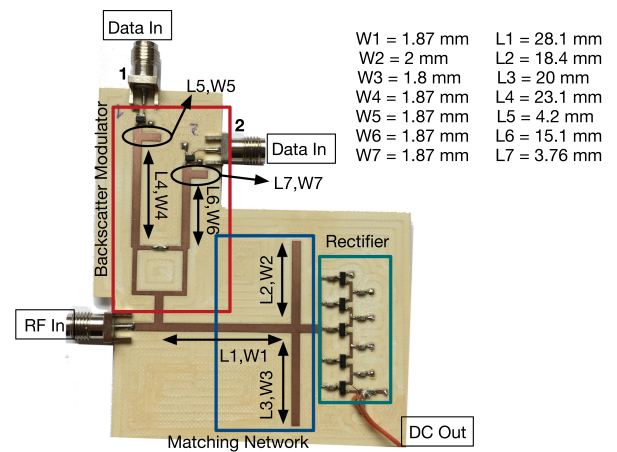

FIGURE 14. System prototype: The system comprises a 16-QAM modulator and a rectifier (substrate for the transmission lines is Astra MT77, thickness = 0.762 mm, ε_r = 3.0, tan δ = 0.0017) and in [115].

shift keying (QPSK) modulator using 4 different impedances selected by 4 RF switches. Furthermore, they also expand their work to a 16-QAM modulator backscatter operating at UHF, where they claim a modulator power consumption of 1.49 mW with a data rate of 96 Mbps as can be seen in [112]. Similarly, this modulator was implemented using 5 switches, and several lumped impedances, being able to recreate a 16-to-1 multiplexer, that operates in 16 different levels, creating the 16-QAM states. The approach followed by [113], was also to implement an I/Q backscatter modulator, in that case, they used two PIN diodes to implement different impedances by controlling the bias currents. The circuit implemented used a Wilkinson power divider combined with two different filters and one PIN diode in each branch to implement the modulator. By using this strategy, they achieved 80 mW, assuming mainly the modulator and not considering any digital counterpart, which clearly is a significant value, if the proposal is to create a passive TAG. Pozar [119] also uses PIN diodes in a reflection-type phase shifter configuration, in that case, two PIN diodes and a quadrature hybrid were used. This configuration works by commuting the diodes in an on-and-off stage, which produces a phase change at the output of the modulator. Nevertheless, the consumption of the PIN diodes shows that this is not a viable solution for passive or semi-passive approaches. Kimionis et al. [120], presented a different approach to developing a binary phase shift keying (BPSK) modulator. The approach follows a phase shift using two different switches connected to different delay lines, one with 0° and another one with 90° delays. By commuting the switches, the delays were changed, and thus the BPSK phase also changed. Finally, the authors in [114] presented a 330 Mb/s of data rate at 2.9 GHz, using BPSK modulation.

Table 4 compares the modulators' results from the provided state-of-the-art references. In [115], the authors have proposed an alternative solution, presented in Fig. 14 divided into two main blocks, the backscatter modulator and an RF-DC
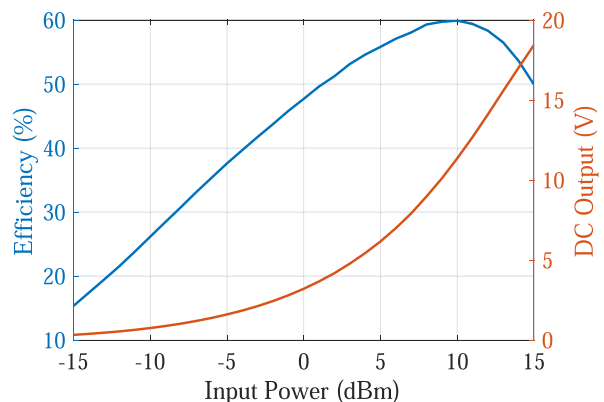
TABLE 4. Performance Summary and Comparison

Reference	[110]	[111]	[112]	[113]	[114]	This work [115]	[116]
Technology	Integrated circuit	Discrete components	Discrete components	Discrete components	Integrated circuit	Discrete components	Integrated circuit
Frequency	5.8 GHz	900 MHz	900 MHz	868 MHz	2.9 GHz	2.45 GHz	10 GHz to 11.1 GHz
Modulation	32-QAM	4-QAM	16-QAM	QAM	BPSK	16-QAM	BPSK
Data rate	2.5 Mb/s	400 kb/s	96 Mb/s	-	330 Mb/s	960 Mb/s	10 Mb/s
Power consumption	113 uW	115 nW	1.4 mW	80 mW	0.12 mW	59 uW	-
Energy p/bit	45.2 pJ/bit	0.29 pJ/bit	15.5 pJ/bit	-	0.36 pJ/bit	61.5 fJ/bit	-
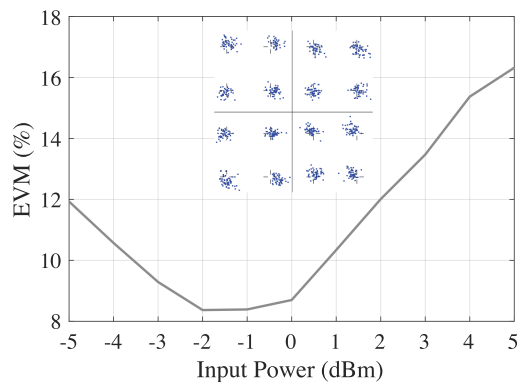
FIGURE 15. Received signal constellation with EVM and energy per bit consumption as a function of input power for 960 Mb/s as in [115].

FIGURE 16. DC output voltage and efficiency as a function of input power at 1.7 GHz with an unbiased gate of each E-pHEMT as in [115].

converter. The first block, the backscatter modulator, is composed of a Wilkinson power divider, two matching networks, and two enhancement-mode high-electron-mobility transistors (E-pHEMTs).

In each branch used, the phases are separated by 45° phase shifts, creating a 90° phase for each of the branch reflected waves. By selecting a different gate voltage at each transistor, we can actually change the impedance seen by the drain, and thus change the reflection coefficient in the Smith chart seen by the antenna. Creating a 16-QAM constellation or even more.

The other block is the RF-DC converter, where the power to energize any microcontroller or sensor can be gathered. This is done using a five-stage Dickson multiplier that is tuned at the WPT frequency, which operates at 1.7 GHz, the backscatter block operates at a different frequency (2.45 GHz). The continuous change of voltage levels at the gate of the transistor will induce different impedances at the input of the rectifier, creating some burden on the simultaneous design of the backscatter and RF-DC converter. The system followed the approach used in [121] by using two different frequencies, one for the backscatter communication and the other for the WPT. When the E-pHEMTs are unbiased, the RF-DC presents 56% of efficiency when 5 dBm of input power is considered. The change in voltage to operate the backscatter block degrades this efficiency, with a worst-case of 10%. The maximum performance achieved with this circuit is represented in Fig. 15, where for a data rate of 960 Mb/s, and an error vector magnitude (EVM) of 8.37% the energy consumption is only 59 μW. For a load of 21.5 kOhm the

average DC output voltage and the overall generated efficiency can be seen in Fig. 16 when the input power is varied. As said above a maximum of 56% efficiency for a 5 dBm input power at 1.7 GHz was obtained when both transistors were unbiased. By using different frequencies for WPT and backscatter, the RF-DC converter can actually behave better for high impedance changes at 2.45 GHz.

The presented prototype circuit works with two different frequencies, one for the WPT link and the other to perform the backscatter communication [115]. This modulator's energy consumption per bit can be as low as 61.5 fJ for a data rate of 960 Mb/s with an EVM of 8.37%. The system has demonstrated some WPT capabilities with 56% of efficiency for an input power of 5 dBm. The presented solution is able to provide high bandwidth solutions for low-power IoT future developments.

B. MILLIMETER WAVE AND SUB-TERAHERTZ BACKSCATTERING

Existing wireless networks are limited in the number of nodes they can concurrently support [122], [123]. Higher frequencies, i.e., millimeter-wave and sub-terahertz bands provide unique opportunities for concurrent transmissions: First, the large spectrum in this regime facilitates dense user populations to operate concurrently at orthogonal frequency channels. Second, narrow-beam directional transmission and reception, which is mandated due to the high path loss, can achieve network scaling by providing opportunities for space division multiple access. Finally, the mm-scale wavelength offers fine-grained localization for future IoT applications.

These frequencies provide the best of the RF and optical spectrum: like RF, they can be phase modulated and experience lower penetration and reflection losses compared with optical while still providing a large swath of continuous bandwidth and laser-shaped beams (just like in optical communication).

Despite these exciting prospects, operation at such a high frequency is fundamentally power-demanding since the power consumption of the RF circuitry is proportional to the frequency. This high power consumption has even stalled the deployment of mobile 28 GHz nodes and will worsen at the 6G and THz regime [124], [125], [126], [127], [128]. Furthermore, directional transmission requires large antenna arrays, which significantly increase the device's power consumption and complexity. This challenge worsens under mobility when constant beam adaption is needed to maintain the link.

Backscatter technology is introduced for energy-efficient communication between power-constrained wireless devices [129], [130]. The underlying idea is to allow low-power nodes to piggyback their data on an ambient signal instead of generating their own RF signal, which would demand power-hungry components such as mixers, oscillators, and amplifiers [131]. Recently, there has been significant work on extending the communication range [132], [133], [134], [135] and improving the data rate of backscatter communication links [136], [137]. In particular, employing low-power coding techniques such as chirp spread spectrum has shown promise for decoding backscattering signals below the noise floor [138]. However, while these techniques can achieve long-range communications, they often do not scale well with the number of devices, i.e., they are often limited to very few (1–2) concurrent links. A recent work [139] allows for concurrent transmission of 256 backscatter devices over a bandwidth of 500 kHz. This work relies on the ability of the low-power nodes to generate cyclically shifted chirps, which is relatively power-demanding. Further, the number of concurrent users is inherently bounded to the bandwidth and the spectral resolution at endpoint devices. Therefore, most existing low-power backscatter solutions have been limited to sub-6 GHz bands [140], [142] as the main challenge of directionality at low power cost remains.

The tags should be *retrodirective* to close a directional link between a mmWave/sub-THz reader and a low-power tag. Retrodirectivity is the capability of a tag to reflect an incident signal toward the source direction without prior knowledge of its direction of arrival. In the literature, there are three methods to achieve retrodirectivity in wireless systems: phase conjugate arrays, Van Atta arrays, and leaky-wave antennas.

Phase conjugate arrays use heterodyne techniques to conjugate the phase of the incoming signal at each antenna element resulting in a radiated beam back toward the source direction. However, such a design requires mixing the impinging RF with a local oscillator [142] at each element, which makes the array bulky, power-hungry, and therefore unsuitable for IoT applications. Recently, the structures like Van Atta Arrays have shown great potential for mmWave backscattering (up to 28 GHz) [137], [143], [144], [145].
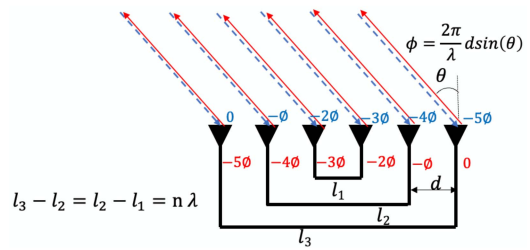
FIGURE 17. Van Atta retro-directive array: This passive multi-antenna architecture reflects any incident wave in reverse, parallel to the direction of incidence, creating a directional link with a reader at zero power cost.

The idea of Van Atta arrays dates back to 1960 [146]. As shown in Fig. 17, they consist of an array of antennas connected in symmetrical pairs by transmission lines. Every antenna in this array serves as receiving and transmitting elements. The signal received by each antenna is transmitted through the line and re-radiates from the corresponding paired antennas. To create an emission pattern that points back to the transmitter, the transmission lines should not contribute other phase differences to incident waves, i.e., they have an equal length or their length differences equal to multiples of the guided wavelength. Further, transmit-receive antenna pairs are deliberately arranged in a mirror-symmetric manner to cause a phase reversal for the reflected beam compared to the incident wavefront.

Unlike phase-conjugated arrays that require active components, Van Atta arrays can be designed entirely with passive components, which makes it well-suited for low-power backscatter. However, the fundamental limitation is that Van Atta Arrays are inherently narrow-band as the transmission lines are optimized at a particular wavelength, which is fixed (non-configurable) after fabrication. In other words, communication bandwidth is inherently limited despite carrier frequencies being in the mmWave regime. The most recent spectrally-agile retrodirective structure is built on a design called leaky-wave antenna [148]. Leaky-wave antennas are waveguides with open slit(s) on one side. Their exciting characteristic is that guided waves can leak out into free space such that the emission angle is correlated with the frequency of the signal [148]. These frequency-dependent radiations have been recently exploited for THz path discovery and localization [149], [150], [152], and have also been demonstrated in CMOS technology [152]. The key insight is that leaky waveguides have reciprocal transmission and reception characteristics. When it acts as a receiver, the impinging signals couple into the waveguide only if their spectral content agrees with the incident angle (i.e., where the angle of emission and reception from the waveguide is frequency-dependent). Hence, by devising two symmetrical slits, one for accepting free-space ambient signals into the waveguide and the other for leaking those signals back into the air, one can enable retrodirectivity. As shown in Fig. 18, an active far-field transceiver emits a THz signal toward the leaky tag. The impinging signal would then couple into the waveguide,
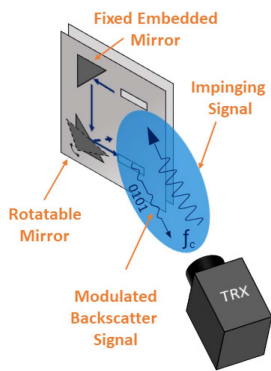
FIGURE 18. Illustrating the retrodirective backscatter link between leaky scatter and a broadband sub-THz transceiver [148].

FIGURE 19. A spiral/dipole integrated antenna for accomplishing UHF energy harvesting and UWB backscattering communication.

which is guided toward the second slit and radiates out back to the free space forming a directional beam that points to the transceiver's location, thereby enabling retrodirectivity. We emphasize that this retrodirective structure is truly wideband and spectrally agile as it can operate between 100 GHz and 500+ GHz. Further, the directionality is achieved with zero power consumption. However, the active transceiver is expected to be power-demanding as it should be capable of generating tunable wideband signals.

C. ULTRA-WIDE-BAND COMMUNICATION

Ultra-wide-band (UWB) communication is one of the best candidates for IoT devices due to its superior robustness for radio channel fading and its intrinsic low-energy requirements. This section describes some available topologies of UWB batteryless tags and their localization performance. Usually, UWB must be coupled with UHF to obtain batteryless operation due to the UWB mask's insufficient low-power constraints to support the energy required for pulse generation. In [154], [154]. a UHF rectenna is integrated with the UWB system for energy harvesting purposes [154], [154]. An energy-autonomous UWB system for localization is presented in [156], where a tag equipped with UHF and UWB is shown; Distributed power sources support its operation at UHF, and anchor nodes at UWB are used for the tag localization. For a sustainable batteryless UWB operation, an integrated co-design of the tag and the antenna front-ends is required to minimize all the possible sources of losses. This includes the nonlinear/EM co-design of the RF sub-systems and antennas and the base-band circuitry for power management purposes. In [156], proofs-of-concept of energy-autonomous UWB tags are designed and tested. The UWB pulse generator is successfully powered by exploiting the WPT sources distributed in the environment. The activation of the whole system has been demonstrated at a 10 m distance with a received RF power of only −13 dB, from cold-start conditions.

We may realize the antenna system by adopting eco-friendly materials to be deployed for massive object monitoring in IoT-like environments. System compactness and
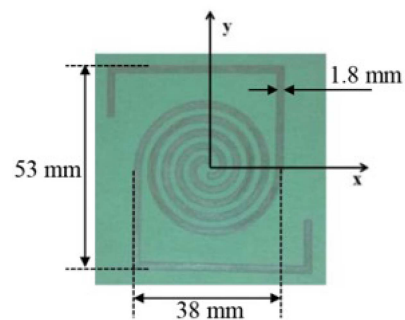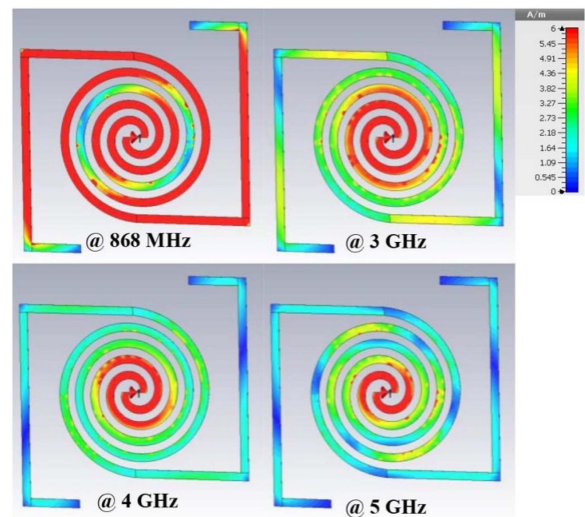

FIGURE 20. Current density distribution over the spiral/dipole antenna at selected operating frequencies.

lightness goals are reached starting from the antenna's implementation, covering both UHF and the European UWB bands [154] with a unique metalization design, using a customized spiral antenna. A prototype of this solution is shown in Fig. 19, where the UHF-UWB operations have been obtained using a modified spiral antenna, acting as a dipole in the UHF band. Representative current distributions at different operating frequencies are shown in Fig. 20, testifying to the predicted operation of the multi-band antenna. To decouple the UHF and UWB operation, a miniaturized duplexer in microstrip technologies has been co-designed with the UWB-UHF antenna to account for the effect of their near-field interactions when the diplexer is integrated into the antenna backplane. In [156], the design and integration of a High Impedance Surface (HIS) into the antenna system allow for insensitivity to the background of the one-port spiral-dipole combination while maintaining a low-profile stack-up structure. This way, the antenna system can be integrated with different materials without affecting its performance. A 3D printing realization increases the structure's robustness and reliability.
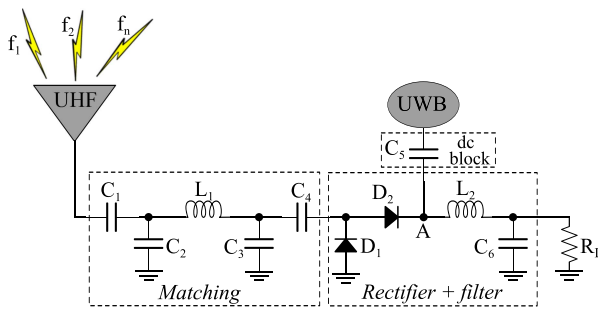
FIGURE 21. Circuit schematic of a chipless UWB tag consisting of a rectenna excited by an optimized multi-sine signal with two output paths, one for collecting DC power and one for backscattering a quasi-UWB pulse consisting of the intermodulation products resulting from the multi-sine excitation.
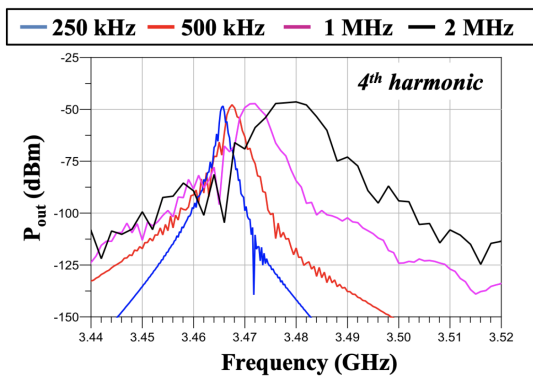
FIGURE 22. Power spectra at the UWB port of the tag of Fig. 21 for different tones spacings and an average input power of −10 dBm.

A chipless UWB/UHF tag with centimeter-level localization has been obtained by a passive generation of a quasi UWB signal, exploiting the nonlinear intermodulation (IM) products generated by the multi-sine excitation of a full-wave rectifier [158]. The rectifier circuit schematic is shown in Fig. 21 and operates in dual mode since its output section consists of two decoupled paths: a DC one, which drives the DC output power into a load (that can be the equivalent circuit of a PMU), optimized for maximum power conversion efficiency; a UWB one which collects the low-power higher harmonics generated by the rectifier to be backscattered as a UWB signal, for passive localization purposes. This architecture has proven to act as a chipless UWB tag (or harmonic UWB tag, since no pulses generations are needed on board) with energy harvesting capabilities. The suitable rectifier/UWB backscatter tag needs to be designed based on the concurrent signal shape optimization of the multi-sine excitations and the rectifier components to simultaneously maximize the harmonic contents of the IM products, flowing to the UWB output path, and the DC power flowing to the DC one. Using a novel, accurate, and efficient harmonic balance simulation set-up, where the multi-tones are represented as the higher harmonics of their frequency spacing, the optimized topology and excitations are straightforwardly derived [158]. Fig. 22 represents the spectral contents of one of the UWB

frequency bands, obtained at the UWB output, as a function of frequency spacing and the number of tones, with a total RF power as low as −10 dBm. The relationship between the UWB signal properties, in terms of bandwidth, the number of tones and tones spacings, and the localization accuracy can be predicted in a very efficient way. The co-designing of the rectifier multi-sine excitation and the quasi-UWB pulse passively generated by exploiting its IM products promises an innovative and attractive solution for future IoT devices that need to combine ultra-low power communication, localization, and sensing. We demonstrated a unique and novel implementation of UWB tags with centimeter-level precision and no need for an onboard UWB pulse generator and the related energy requirements.

V. CONCLUSION

This paper discusses eco-friendly manufacturing, sustainable powering, and wireless connectivity for next-generation IoT devices to ensure that IoT technology can sustainably grow to be a part of the future connected world. Sustainable IoT devices are enabled by addressing environmental concerns using eco-friendly materials, reducing carbon footprints, and removing toxic materials from the manufacturing processes. Sustainable IoT devices are also enabled by exploiting energy harvesting and wireless power transfer technologies to eliminate the eco-toxicity of batteries or, if it is impossible to operate without a battery fully, to reduce the cost of battery replacement. Another enabler of sustainable IoT devices is novel wireless connectivity solutions compatible with batteryless operation and energy harvesting schemes as, for example, retroreflective connectivity in the millimeter wave bands and beyond, higher-order modulation schemes, and wideband communication to improve the data rate and user density in the backscatter networks.

Throughout the article, we present unique design solutions providing sustainable IoT devices in one or more aspects of reaching sustainability. For example, we present backscatter IoT devices that rely on a wireless power transfer from the interrogator device, provide a batteryless operation, and are realized on an eco-friendly substrate material. However, there are many more aspects of sustainability than we have presented, e.g., sustainability issues of IoT devices on a societal level regarding the security and privacy of data. Thus, to reach fully sustainable IoT solutions, RF engineers have to team up with researchers from other disciplines. We also envision increasing interdisciplinary research efforts to address the further-increasing design requirements of IoT devices, e.g., by teaming up with computer scientists and exploring tiny artificial intelligence algorithms to provide reliable wireless communication in harsh propagation environments.

REFERENCES

[1] Qualcomm Inc., "Intelligently connecting our world in the 5G era," May 2020. [Online]. Available: https://www.qualcomm.com/content/dam/qcomm-martech/dm-assets/documents/intelligently_connecting_our_world_in_the_5g_era_web_1.pdf

[2] H. Rahmani et al., "Towards a machine-learning-assisted dielectric sensing platform for point-of-care wound monitoring," *IEEE Sens. Lett.*, vol. 4, no. 6, Jun. 2020, Art. no. 5501004.

[3] J. Jang, I. Habibagahi, H. Rahmani, and A. Babakhani, "Wirelessly powered, batteryless closed-loop biopotential recording ic for implantable leadless cardiac monitoring applications," in *Proc. IEEE Biomed. Circuits Syst. Conf.*, 2021, pp. 1–4.

[4] M. J. Tan, C. Owh, P. L. Chee, A. K. K. Kyaw, D. Kai, and X. J. Loh, "Biodegradable electronics: Cornerstone for sustainable electronics and transient applications," *J. Mater. Chem. C*, vol. 4, no. 24, pp. 5531–5558, Jun. 2016. [Online]. Available: https://pubs.rsc.org/en/content/articlelanding/2016/tc/c6tc00678g

[5] M. Chakraborty, J. Kettle, and R. Dahiya, "Electronic waste reduction through devices and printed circuit boards designed for circularity," *IEEE J. Flexible Electron.*, vol. 1, no. 1, pp. 4–23, Jan. 2022.

[6] "A new circular vision for electronics time for a global reboot," Jan. 2019. Accessed: Aug. 8, 2022. [Online]. Available: https://www3.weforum.org/docs/WEF_A_New_Circular_Vision_for_Electronics.pdf

[7] V. Forti, C. P. Balde, R. Kuehr, and G. Bel, *The Global E-Waste Monitor 2020: Quantities, Flows and the Circular Economy Potential.* Bonn, Geneva and Rotterdam: United Nations Univ./United Nations Instit. Training Res., Int. Telecommun. Union, Int. Solid Waste Assoc., Jul. 2020. [Online]. Available: https://collections.unu.edu/view/UNU:7737

[8] E. Long, S. Kokke, D. Lundie, N. Shaw, W. Ijomah, and C.-C. Kao, "Technical solutions to improve global sustainable management of waste electrical and electronic equipment (WEEE) in the EU and China," *J. Remanufacturing*, vol. 6, no. 1, pp. 1–27, Jan. 2016. [Online]. Available: https://doi.org/10.1186/s13243-015-0023-6

[9] Y. Sui, M. Atreya, S. Dahal, A. Gopalakrishnan, R. Khosla, and G. L. Whiting, "Controlled biodegradation of an additively fabricated capacitive soil moisture sensor," *ACS Sustain. Chem. Eng.*, vol. 9, no. 6, pp. 2486–2495, Feb. 2021. [Online]. Available: https://pubs.acs.org/doi/10.1021/acssuschemeng.0c07615

[10] M. Wagih, Y. Wei, A. Komolafe, R. Torah, and S. Beeby, "Reliable UHF long-range textile-integrated RFID tag based on a compact flexible antenna filament," *Sensors*, vol. 20, no. 12, 2020, Art. no. 3435.

[11] B. S. Cook, J. R. Cooper, and M. M. Tentzeris, "Multi-layer RF capacitors on flexible substrates utilizing inkjet printed dielectric polymers," *IEEE Microw. Wireless Compon. Lett.*, vol. 23, no. 7, pp. 353–355, Jul. 2013.

[12] M. Wagih, A. Komolafe, and N. Hillier, "Screen-printable flexible textile-based ultra-broadband millimeter-wave DC-blocking transmission lines based on microstrip-embedded printed capacitors," *IEEE J. Microwaves*, vol. 2, no. 1, pp. 162–173, Jan. 2022.

[13] M. Wagih, G. S. Hilton, A. S. Weddell, and S. Beeby, "Dual-band dual-mode textile antenna/rectenna for simultaneous wireless information and power transfer (SWIPT)," *IEEE Trans. Antennas Propag.*, vol. 69, no. 10, pp. 6322–6332, Oct. 2021.

[14] M. Wagih, N. Hillier, S. Yong, A. S. Weddell, and S. Beeby, "RF-powered wearable energy harvesting and storage module based on e-textile coplanar waveguide rectenna and supercapacitor," *IEEE Open J. Antennas Propag.*, vol. 2, pp. 302–314, 2021.

[15] S. Lemey, S. Agneessens, P. V. Torre, K. Baes, J. Vanfleteren, and H. Rogier, "Wearable flexible lightweight modular RFID tag with integrated energy harvester," *IEEE Trans. Microw. Theory Techn.*, vol. 64, no. 7, pp. 2304–2314, Jul. 2016.

[16] Y. H. Jung et al., "High-performance green flexible electronics based on biodegradable cellulose nanofibril paper," *Nature Commun.*, vol. 6, no. 1, May 2015, Art. no. 7170. [Online]. Available: https://doi.org/10.1038/ncomms8170

[17] S.-W. Hwang et al., "Materials for bioresorbable radio frequency electronics," *Adv. Mater.*, vol. 25, no. 26, pp. 3526–3531, 2013.

[18] C. Hoyer et al., "Bendable 190-GHz transmitter on 20-μm ultra-thin SiGe BiCMOS," *IEEE J. Flexible Electron.*, vol. 1, no. 2, pp. 122–133, Feb. 2022.

[19] M. Wagih, S. Yong, K. Yang, A. S. Weddell, and S. Beeby, "Printed non-metallic textile-based carbon antenna for low-cost green wearable applications," in *Proc. 16th Eur. Conf. Antennas Propag.*, 2022, pp. 1–4.

[20] Z. Li et al., "All-organic flexible fabric antenna for wearable electronics," *J. Mater. Chem. C*, vol. 8, pp. 5662–5667, 2020.

[21] S. J. Chen et al., "A compact, highly efficient and flexible polymer ultra-wideband antenna," *IEEE Antennas Wireless Propag. Lett.*, vol. 14, pp. 1207–1210, 2015.

[22] R. J. Hernandez, C. Miranda, and J. Goñi, "Empowering sustainable consumption by giving back to consumers the 'right to repair'," *Sustainability*, vol. 12, no. 3, Jan. 2020, Art. no. 850. [Online]. Available: https://www.mdpi.com/2071-1050/12/3/850

[23] V. Palazzi, S. Bonafoni, F. Alimenti, P. Mezzanotte, and L. Roselli, "Feeding the world with microwaves: How remote and wireless sensing can help precision agriculture," *IEEE Microw. Mag.*, vol. 20, no. 12, pp. 72–86, Dec. 2019.

[24] F. Alimenti, P. Mezzanotte, M. Dionigi, M. Virili, and L. Roselli, "Microwave circuits in paper substrates exploiting conductive adhesive tapes," *IEEE Microw. Compon. Lett.*, vol. 22, no. 12, pp. 660–662, Dec. 2012.

[25] V. Palazzi, F. Alimenti, D. Zito, P. Mezzanotte, and L. Roselli, "A 24-GHz single-transistor oscillator on paper," *IEEE Microw. Compon. Lett.*, vol. 30, no. 11, pp. 1085–1088, Nov. 2020.

[26] R. Gonçalves et al., "RFID-based wireless passive sensors utilizing cork materials," *IEEE Sensors J.*, vol. 15, no. 12, pp. 7242–7251, Dec. 2015.

[27] G. Boussatour, P.-Y. Cresson, B. Genestie, N. Joly, and T. Lasri, "Dielectric characterization of polylactic acid substrate in the frequency band 0.5–67 GHz," *IEEE Microw. Compon. Lett.*, vol. 28, no. 5, pp. 374–376, May 2018.

[28] S. B. Bon et al., "Self-adhesive plasticized regenerated silk on poly (3-hydroxybutyrate-co-3-hydroxyvalerate) for bio-piezoelectric force sensor and microwave circuit design," *J. Appl. Polym. Sci.*, vol. 138, no. 4, 2021, Art. no. 49726.

[29] V. Palazzi, F. Alimenti, P. Mezzanotte, G. Orecchini, and L. Roselli, "Zero-power, long-range, ultra low-cost harmonic wireless sensors for massively distributed monitoring of cracked walls," in *Proc. IEEE MTT-S Int. Microw. Symp.*, 2017, pp. 1335–1338.

[30] A. M. J. Marindra and G. Y. Tian, "Chipless RFID sensor tag for metal crack detection and characterization," *IEEE Trans. Microw. Theory Techn.*, vol. 66, no. 5, pp. 2452–2462, May 2018.

[31] N. Javed, M. Azam, and Y. Amin, "Chipless RFID multisensor for temperature sensing and crack monitoring in an IoT environment," *IEEE Sens. Lett.*, vol. 5, no. 6, Jun. 2021, Art. no. 6001404.

[32] C. Cho, X. Yi, D. Li, Y. Wang, and M. M. Tentzeris, "Passive wireless frequency doubling antenna sensor for strain and crack sensing," *IEEE Sensors J.*, vol. 16, no. 14, pp. 5725–5733, Jul. 2016.

[33] P. Kalansuriya, R. Bhattacharyya, and S. Sarma, "RFID tag antenna-based sensing for pervasive surface crack detection," *IEEE Sensors J.*, vol. 13, no. 5, pp. 1564–1570, May 2013.

[34] S. Dey, P. Kalansuriya, and N. C. Karmakar, "Novel chipless RFID high resolution crack sensor based on SWB technology," *IEEE Sensors J.*, vol. 21, no. 3, pp. 2908–2920, Feb. 2021.

[35] S. Caizzone, E. DiGiampaolo, and G. Marrocco, "Wireless crack monitoring by stationary phase measurements from coupled RFID tags," *IEEE Trans. Antennas Propag.*, vol. 62, no. 12, pp. 6412–6419, Dec. 2014.

[36] J. Zhang, B. Huang, G. Zhang, and G. Y. Tian, "Wireless passive ultra high frequency RFID antenna sensor for surface crack monitoring and quantitative analysis," *Sensors*, vol. 18, no. 7, 2018, Art. no. 2130.

[37] F. Alimenti et al., "A wireless MEMS humidity sensor based on a paper-aluminium bimorph cantilever," in *Proc. IEEE MTT-S Int. Microw. Symp.*, 2021, pp. 823–826.

[38] Z. Lu et al., "Highly flexible and transparent polylactic acid composite electrode for perovskite solar cells," *Sol. RRL*, vol. 4, no. 10, 2020, Art. no. 2000320.

[39] F. Alimenti et al., "24-GHz CW radar front-ends on cellulose-based substrates: A new technology for low-cost applications," in *Proc. IEEE MTT-S Int. Microw. Symp.*, 2015, pp. 1–4.

[40] F. Alimenti et al., "A 24-GHz front-end integrated on a multilayer cellulose-based substrate for doppler radar sensors," *Sensors*, vol. 17, no. 9, 2017, Art. no. 2090.

[41] H. L. Lee, W.-G. Lim, K.-S. Oh, and J.-W. Yu, "24 GHz balanced Doppler radar front-end with Tx leakage canceller for antenna impedance variation and mutual coupling," *IEEE Trans. Antennas Propag.*, vol. 59, no. 12, pp. 4497–4504, Dec. 2011.

[42] H.-S. Lee and C.-Y. Kim, "An LTCC multilayer packaged 24-GHz short-range radar with an embeded Tx leakage canceller," *Microw. Opt. Tech. Lett.*, vol. 56, no. 3, pp. 671–677, 2014.

[43] "24 GHz radar sensor, IMST GmbH," 2017. [Online]. Available: http://www.imst.de

[44] "K-LC5-High sensitivity dual channel transceiver, RFbeam microwave GmbH," 2017. [Online]. Available: https://www.rfbeam.ch/files/products/9/downloads/Datasheet_K-LC5.pdf

[45] F. Alimenti et al., "A low-cost 24 GHz Doppler radar sensor for traffic monitoring implemented in standard discrete-component technology," in *Proc. Eur. Microw. Conf.*, 2007, pp. 1441–1444.

[46] F. Alimenti et al., "24-GHz CW radar front-ends on cellulose-based substrates: A new technology for low-cost applications," in *Proc. IEEE MTT-S Int. Microw. Symp.*, 2015, pp. 1–4.

[47] "Silicon germanium 24 GHz radar transceiver MMIC, infineon technologies AG," Datasheet, Revision 1.3, May 8, 2018. [Online]. Available: https://www.infineon.com/dgdl/Infineon-BGT24LTR11N16-DataSheet-v01_03-EN.pdf?fileId=5546d4625696ed7601569d2ae3a9158a

[48] M. Virili et al., "7.5–15 MHz organic frequency doubler made with pentacene-based diode and paper substrate," in *Proc. IEEE MTT-S Int. Microw. Symp.*, 2014, pp. 1–4, doi: 10.1109/MWSYM.2014.6848395.

[49] B. J. Kim et al., "Highly efficient and bending durable perovskite solar cells: Toward a wearable power source," *Energy Environ. Sci.*, vol. 8, no. 3, pp. 916–921, 2015.

[50] S. Seok, C. Wang, E. Lefeuvre, and J. Park, "Autonomous energy harvester based on textile-based enzymatic biofuel cell for on-demand usage," *Sensors*, vol. 20, no. 17, 2020, Art. no. 5009.

[51] H. Y. Alkhalaf, M. Y. Ahmad, and H. Ramiah, "Self-sustainable biomedical devices powered by RF energy: A review," *Sensors*, vol. 22, no. 17, 2022, Art. no. 6371.

[52] S. Castro-Hermosa, G. Lucarelli, M. Top, M. Fahland, J. Fahlteich, and T. M. Brown, "Perovskite photovoltaics on roll-to-roll coated ultra-thin glass as flexible high-efficiency indoor power generators," *Cell Rep. Phys. Sci.*, vol. 1, no. 5, 2020, Art. no. 100045.

[53] H. Sharma, A. Haque, and Z. A. Jaffery, "Solar energy harvesting wireless sensor network nodes: A survey," *J. Renewable Sustain. Energy*, vol. 10, no. 2, 2018, Art. no. 023704.

[54] S. Yan et al., "Eggshell membrane and expanded polytetrafluoroethylene piezoelectric-enhanced triboelectric bio-nanogenerators for energy harvesting," *Int. J. Energy Res.*, vol. 45, no. 7, pp. 11053–11064, 2021.

[55] C. Cho, B. Kim, S. Park, and E. Kim, "Bisulfate transport in hydrogels for self-healable and transparent thermoelectric harvesting films," *Energy Environ. Sci.*, vol. 15, no. 5, pp. 2049–2060, 2022.

[56] G. Zhou, L. Huang, W. Li, and Z. Zhu, "Harvesting ambient environmental energy for wireless sensor networks: A survey," *IEEE J. Sensors*, vol. 2014, 2014, Art. no. 815467

[57] J. W. Matiko, N. J. Grabham, S. P. Beeby, and M. J. Tudor, "Review of the application of energy harvesting in buildings," *Meas. Sci. Technol.*, vol. 25, no. 1, 2013, Art. no. 012002.

[58] P. Visconti, P. Primiceri, R. Ferri, M. Pucciarelli, and E. Venere, "An overview on state-of-art energy harvesting techniques and choice criteria: A WSN node for goods transport and storage powered by a smart solar-based eh system," *Int. J. Renewable Energy Res*, vol. 7, pp. 1281–1295, 2017.

[59] A. Thakre, A. Kumar, H.-C. Song, D.-Y. Jeong, and J. Ryu, "Pyroelectric energy conversion and its applications–flexible energy harvesters and sensors," *Sensors*, vol. 19, no. 9, 2019, Art. no. 2170.

[60] Y. Wu, J. Qu, W. A. Daoud, L. Wang, and T. Qi, "Flexible composite-nanofiber based piezo-triboelectric nanogenerators for wearable electronics," *J. Mater. Chem. A*, vol. 7, no. 21, pp. 13347–13355, 2019.

[61] J. He et al., "Piezoelectric-enhanced triboelectric nanogenerator fabric for biomechanical energy harvesting," *Nano Energy*, vol. 64, 2019, Art. no. 103933.

[62] Z. Song et al., "Enhanced energy harvesting performance of triboelectric nanogenerator via efficient dielectric modulation dominated by interfacial interaction," *Nano Energy*, vol. 92, 2022, Art. no. 106759.

[63] H. Zhang et al., "Enhanced performance triboelectric nanogenerator based on porous structure C/MnO$_2$ nanocomposite for energy harvesting," *Nano Res.*, vol. 15, pp. 7163–7171, 2022.

[64] D. Vital, S. Bhardwaj, and J. L. Volakis, "Textile-based large area RF-power harvesting system for wearable applications," *IEEE Trans. Antennas Propag.*, vol. 68, no. 3, pp. 2323–2331, Mar. 2020.

[65] D. Vital, P. Gaire, S. Bhardwaj, and J. L. Volakis, "An ergonomic wireless charging system for integration with daily life activities," *IEEE Trans. Microw. Theory Techn.*, vol. 69, no. 1, pp. 947–954, Jan. 2020.

[66] E. Kwiatkowski, J. A. Estrada, A. López-Yela, and Z. Popović, "Broadband RF energy-harvesting arrays," *Proc. IEEE*, vol. 110, no. 1, pp. 74–88, Jan. 2022.

[67] M. Wagih, A. S. Weddell, and S. Beeby, "Omnidirectional dual-polarized low-profile textile rectenna with over 50% efficiency for sub-μw/cm^2 wearable power harvesting," *IEEE Trans. Antennas Propag.*, vol. 69, no. 5, pp. 2522–2536, May 2020.

[68] X. Huang et al., "Wearable biofuel cells based on the classification of enzyme for high power outputs and lifetimes," *Biosensors Bioelectron.*, vol. 124, pp. 40–52, 2019.

[69] Y. Cao et al., "A full-textile triboelectric nanogenerator with multisource energy harvesting capability," *Energy Convers. Manage.*, vol. 267, 2022, Art. no. 115910.

[70] J. Katic, S. Rodriguez, and A. Rusu, "A high-efficiency energy harvesting interface for implanted biofuel cell and thermal harvesters," *IEEE Trans. Power Electron.*, vol. 33, no. 5, pp. 4125–4134, May 2018.

[71] O. L. López, H. Alves, R. D. Souza, S. Montejo-Sánchez, E. M. G. Fernández, and M. Latva-Aho, "Massive wireless energy transfer: Enabling sustainable IoT toward 6G era," *IEEE Internet Things J.*, vol. 8, no. 11, pp. 8816–8835, Nov. 2021.

[72] M.-L. Ku, W. Li, Y. Chen, and K. J. Ray Liu, "Advances in energy harvesting communications: Past, present, and future challenges," *IEEE Commun. Surv. Tuts.*, vol. 18, no. 2, pp. 1384–1412, Feb. 2016.

[73] K. Elouarzaki, D. Cheng, A. C. Fisher, and J.-M. Lee, "Coupling orientation and mediation strategies for efficient electron transfer in hybrid biofuel cells," *Nature Energy*, vol. 3, no. 7, pp. 574–581, 2018.

[74] Z. Yu et al., "Nanoporous PVDF hollow fiber employed piezo–tribo nanogenerator for effective acoustic harvesting," *ACS Appl. Mater. Interfaces*, vol. 13, no. 23, pp. 26981–26988, 2021.

[75] T. Qin et al., "Asymmetric sulfonyldibenzene-based hole-transporting materials for efficient perovskite solar cells: Inspiration from organic thermally-activated delayed fluorescence molecules," *ACS Mater. Lett.*, vol. 2, no. 9, pp. 1093–1100, 2020.

[76] H. Rahmani and A. Babakhani, "An integrated battery-less wirelessly powered RFID tag with clock recovery and data transmitter for UWB localization," in *IEEE MTT-S Int. Microw. Symp. Dig.*, 2020, pp. 1–4.

[77] A. A. Khan, A. Mahmud, and D. Ban, "Evolution from single to hybrid nanogenerator: A contemporary review on multimode energy harvesting for self-powered electronics," *IEEE Trans. Nanotechnol.*, vol. 18, pp. 21–36, 2019.

[78] H. Rahmani and A. Babakhani, "A fully integrated electromagnetic energy harvesting circuit with an on-chip antenna for biomedical implants in 180 nm SOI CMOS," in *Proc. IEEE SENSORS*, 2016, pp. 1–3.

[79] B. Zhao, N. Kuo, B. Liu, Y. Li, L. Iotti, and A. M. Niknejad, "A 5.8 GHz power-harvesting 116 μm × 116 μm "dielet" near-field radio with on-chip coil antenna," in *IEEE Int. Solid-State Circuits Conf. Dig. Tech. Papers*, 2018, pp. 456–458.

[80] H. Rahmani, Y. Sun, M. Kherwa, S. Pal, and A. Babakhani, "Coherent radiation from a swarm of wirelessly powered and synchronized sensor nodes," *IEEE Sensors J.*, vol. 20, no. 19, pp. 11608–11616, Oct. 2020.

[81] J. Grosinger and A. Michalowska-Forsyth, "Space tags: Ultra-low-power operation and radiation hardness for passive wireless sensor tags," *IEEE Microw. Mag.*, vol. 23, no. 3, pp. 55–71, Mar. 2022.

[82] L.-G. Tran, H.-K. Cha, and W.-T. Park, "RF power harvesting: A review on designing methodologies and applications," *Micro Nano Syst., Lett.*, vol. 5, no. 1, pp. 1–16, Mar. 2017.

[83] D. Shetty, C. Steffan, G. Holweg, W. Bösch, and J. Grosinger, "Submicrowatt CMOS rectifier for a fully passive wake-up receiver," *IEEE Trans. Microw. Theory Techn.*, vol. 69, no. 11, pp. 4803–4812, Nov. 2021.

[84] D. Shetty, C. Steffan, W. Bösch, and J. Grosinger, "Sub-GHz RF energy harvester including a small loop antenna," in *Proc. IEEE Asian Solid-State Circuits Conf.*, 2022, pp. 1–3.

[85] L. Zöscher, P. Herkess, J. Grosinger, U. Mühlmann, D. Amschl, and W. Bösch, "Passive differential UHF RFID front-ends in a 40 nm CMOS technology," in *Proc. 47th Eur. Microw. Conf.*, 2017, pp. 105–108.

[86] Z. Zeng et al., "Design of sub-gigahertz reconfigurable RF energy harvester from −22 to 4 dBm with 99.8% peak MPPT power efficiency," *IEEE J. Solid-State Circuits*, vol. 54, no. 9, pp. 2601–2613, Sep. 2019.

[87] S. M. Noghabaei, R. L. Radin, Y. Savaria, and M. Sawan, "A high-sensitivity wide input-power-range ultra-low-power RF energy," *IEEE Trans. Circuits Syst. I, Reg. Papers*, vol. 69, no. 1, pp. 440–451, Jan. 2022.

[88] P. Saffari, A. Basaligheh, and K. Moez, "An RF-to-DC rectifier with high efficiency over wide input power range for RF energy harvesting applications," *IEEE Trans. Circuits Syst. I., Reg. Papers*, vol. 66, no. 12, pp. 4862–4875, Dec. 2019.

[89] M. Stoopman, S. Keyrouz, H. J. Visser, K. Philips, and W. A. Serdijn, "Co-design of a CMOS rectifier and small loop antenna for highly sensitive RF energy harvesters," *IEEE J. Solid-State Circuits*, vol. 49, no. 3, pp. 622–634, Mar. 2014.

[90] M. A. Abouzied, K. Ravichandran, and E. Sánchez-Sinencio, "A fully integrated reconfigurable self-startup RF energy-harvesting system with storage capability," *IEEE J. Solid-State Circuits*, vol. 52, no. 3, pp. 704–719, Mar. 2017.

[91] Z. Hameed and K. Moez, "A 3.2 V −15 dBm adaptive threshold-voltage compensated RF energy harvester in 130 nm CMOS," *IEEE Trans. Circuits Syst. I, Reg. Papers*, vol. 62, no. 4, pp. 948–956, Apr. 2015.

[92] G. Papotto, F. Carrara, and G. Palmisano, "A 90-nm CMOS threshold-compensated RF energy harvester," *IEEE J. Solid-State Circuits*, vol. 46, no. 9, pp. 1985–1997, Sep. 2011.

[93] S. Schmickl, T. Faseth, and H. Pretl, "An RF-energy harvester and IR-UWB transmitter for ultra-low-power battery-less biosensors," *IEEE Trans. Circuits Syst. I, Reg. Papers*, vol. 67, no. 5, pp. 1459–1468, May 2020.

[94] P. Xu, D. Flandre, and D. Bol, "A self-gating RF energy harvester for wireless power transfer with high-PAPR incident waveform," *IEEE J. Solid State Circuits*, vol. 56, no. 6, pp. 1816–1826, Jun. 2021.

[95] S. Oh, N. E. Roberts, and D. D. Wentzloff, "A 116 nW multi-band wake-up receiver with 31-bit correlator and interference rejection," in *Proc. IEEE Custom Integr. Circuits Conf.*, 2013, pp. 1–4.

[96] P. Chen, T.-K. Chen, Y.-S. Wang, and C.-C. Chen, "A time-domain sub-micro watt temperature sensor with digital set-point programming," *IEEE Sensors J.*, vol. 9, no. 12, pp. 1639–1646, Dec. 2009.

[97] D. Shetty, C. Steffan, W. Bösch, and J. Grosinger, "Ultra-low-power IoT 30 nW 474 mV 19 ppm/°C voltage reference and 2 nA 470 ppm/°C current reference," in *Proc. IEEE Int. Symp. Circuits Syst.*, 2022, pp. 843–847.

[98] D. Shetty, C. Steffan, G. Holweg, W. Bösch, and J. Grosinger, "Ultra-low-power sub-1 V 29 ppm /° C voltage reference and shared-resistive current reference," *IEEE Trans. Circuits Syst. I, Reg. Papers*, early access, Dec. 06, 2022, doi: 10.1109/TCSI.2022.3225574.

[99] J. Grosinger, W. Pachler, and W. Bösch, "Tag size matters: Miniaturized RFID tags to connect smart objects to the internet," *IEEE Microw. Mag.*, vol. 19, no. 6, pp. 101–111, Sep.–Oct. 2018.

[100] L. J. Görtschacher and J. Grosinger, "UHF RFID sensor system using tag signal patterns: Prototype system," *IEEE Antennas Wireless Propag. Lett.*, vol. 18, no. 10, pp. 2209–2213, Oct. 2019.

[101] H. Rahmani and A. Babakhani, "A dual-mode RF power harvesting system with an on-chip coil in 180-nm SOI CMOS for millimeter-sized biomedical implants," *IEEE Trans. Microw. Theory Techn.*, vol. 67, no. 1, pp. 414–428, Jan. 2019.

[102] A. S. Y. Poon, S. O'Driscoll, and T. H. Meng, "Optimal frequency for wireless power transmission into dispersive tissue," *IEEE Trans. Antennas Propag.*, vol. 58, no. 5, pp. 1739–1750, May 2010.

[103] H. Rahmani and A. Babakhani, "A wireless power receiver with an on-chip antenna for millimeter-size biomedical implants in 180 nm SOI CMOS," in *Proc. IEEE MTT-S Int. Microw. Symp.*, 2017, pp. 300–303.

[104] E. Falkenstein, M. Roberg, and Z. Popovic, "Low-power wireless power delivery," *IEEE Trans. Microw. Theory Techn.*, vol. 60, no. 7, pp. 2277–2286, Jul. 2012.

[105] H. Rahmani and A. Babakhani, "A 434 MHz dual-mode power harvesting system with an on-chip coil in 180 nm CMOS SOI for mm-sized implants," in *IEEE MTT-S Int. Microw. Symp. Dig.*, 2018, pp. 1130–1133.

[106] K. N. Bocan and E. Sejdić, "Adaptive transcutaneous power transfer to implantable devices: A state of the art review," *Sensors*, vol. 16, no. 3, 2016, Art. no. 393.

[107] H. Rahmani and A. Babakhani, "A 1.6 mm^3 wirelessly powered reconfigurable FDD radio with on-chip antennas achieving 4.7 pJ/b TX and 1 pJ/b RX energy efficiencies for medical implants," in *Proc. IEEE Custom Integr. Circuits Conf.*, 2020, pp. 1–4.

[108] J. Ding, M. Nemati, C. Ranaweera, and J. Choi, "IoT connectivity technologies and applications: A survey," *IEEE Access*, vol. 8, pp. 67646–67673, 2020.

[109] H. Rahmani and A. Babakhani, "A wirelessly powered reconfigurable FDD radio with on-chip antennas for multi-site neural interfaces," *IEEE J. Solid-State Circuits*,, vol. 56, no. 10, pp. 3177–3190, Oct. 2021.

[110] A. Shirane et al., "13.8 A. 5.8 GHz RF-powered transceiver with a 113 μW 32-QAM transmitter employing the IF-based quadrature backscattering technique," in *Proc. IEEE Int. Solid-State Circuits Conf. Dig. Tech. Paper*, 2015, pp. 1–3.

[111] S. J. Thomas, E. Wheeler, J. Teizer, and M. S. Reynolds, "Quadrature amplitude modulated backscatter in passive and semipassive UHF RFID systems," *IEEE Trans. Microw. Theory Techn.*, vol. 60, no. 4, pp. 1175–1182, Apr. 2012.

[112] S. J. Thomas and M. S. Reynolds, "A 96 Mbit/sec, 15.5 pJ/bit 16-QAM modulator for UHF backscatter communication," in *Proc. IEEE Int. Conf. RFID*, 2012, pp. 185–190.

[113] M. Winkler, T. Faseth, H. Arthaber, and G. Magerl, "An UHF RFID tag emulator for precise emulation of the physical layer," *Proc. Microw. Conf.*, 2010, pp. 273–276.

[114] A. Tang, Y. Kim, and M.-C. F. Chang, "A 65 nm CMOS 330 Mb/s microwave backscatter link at 2.4 to 2.9 GHz with ambient blocker cancellation," *IEEE Microw. Wireless Compon. Lett.*, vol. 26, no. 1, pp. 61–63, Jan. 2016.

[115] R. Correia and N. B. Carvalho, "Ultrafast backscatter modulator with low-power consumption and wireless power transmission capabilities," *IEEE Microw. Wireless Compon. Lett.*, vol. 27, no. 12, pp. 1152–1154, Dec. 2017.

[116] X. Fu, A. Sharma, E. Kampianakis, A. Pedross-Engel, D. Arnitz, and M. S. Reynolds, "A low cost 10.0–11.1 GHz X-band microwave backscatter communication testbed with integrated planar wideband antennas," in *Proc. IEEE Int. Conf. RFID*, 2016, pp. 1–4.

[117] R. Correia, P. Pinho, and N. Carvalho, "Backscatter radio communication for IoT applications," *I-ETC: ISEL Academic J. Electron. Telecommun. Comput.*, vol. 4, no. 1, 2018, Art. no. 2.

[118] S. Thomas and M. S. Reynolds, "QAM Backscatter for Passive UHF RFID Tags," in *Proc. IEEE Int. Conf. RFID*, 2010, pp. 210–214.

[119] D. M. Pozar, *Microwave Engineering*. Hoboken, NJ, USA: Wiley, 2012.

[120] J. Kimionis and M. M. Tentzeris, "Pulse shaping for backscatter radio," in *Proc. IEEE MTT-S Int. Microw. Symp*, 2016, pp. 1–4.

[121] R. Correia, N. B. Carvalho, and S. Kawasaki, "Continuously power delivering for passive backscatter wireless sensor networks," *IEEE Trans. Microw. Theory Techn.*, vol. 64, no. 11, pp. 3723–3731, Nov. 2016.

[122] Q. Liang, T. S. Durrani, X. Gu, J. Koh, Y. Li, and X. Wang, "Guest editorial special issue on spectrum and energy efficient communications for Internet of Things," *IEEE Internet Things J.*, vol. 6, no. 4, pp. 5948–5953, Apr. 2019.

[123] Federal Communications Commission, "The commission seeks comment on spectrum for the Internet of Things," ET Docket, no. 21-353, Sep. 9, 2021. [Online]. Available: https://www.google.com/url?sa=t&rct=j&q=&esrc=s&source=web&cd=&ved=2ahUKEwiN_sD-qoj8AhWNhP0HHW2TACgQFnoECBIQAQ&url=https%3A%2F%2Fdocs.fcc.gov%2Fpublic%2Fattachments%2FDOC-375610A1.pdf&usg=AOvVaw2bL_1lRySESUEhCdp5UK6v

[124] S. Dutta, C. N. Barati, D. Ramirez, A. Dhananjay, J. F. Buckwalter, and S. Rangan, "A case for digital beamforming at mmWave," *IEEE Trans. Wireless Commun.*, vol. 19, no. 2, pp. 756–770, Feb. 2019.

[125] P. Skrimponis et al., "Power consumption analysis for mobile mmWave and sub-THz receivers," in *Proc. 2nd 6G Wireless Summit*, 2020, pp. 1–5.

[126] S. Rangan, T. S. Rappaport, and E. Erkip, "Millimeter-wave cellular wireless networks: Potentials and challenges," *Proc. IEEE*, vol. 102, no. 3, pp. 366–385, Mar. 2014.

[127] T. S. Rappaport et al., "Millimeter wave mobile communications for 5G Cellular: It will work!," *IEEE Access*, vol. 1, pp. 335–349, 2013.

[128] T. S. Rappaport, R. W. Heath Jr., R. C. Daniels, and J. N. Murdock, *Millimeter Wave Wireless Communications*. London, U.K.: Pearson, 2015.

[129] C. Boyer and S. Roy, "Backscatter communication and RFID: Coding, energy, and MIMO analysis," *IEEE Trans. Commun.*, vol. 62, no. 3, pp. 770–785, Mar. 2014.

[130] E. Ilie-Zudor, Z. Kemény, F. V. Blommestein, L. Monostori, and A. V. D. Meulen, "A survey of applications and requirements of unique identification systems and RFID techniques," *Comput. Ind.*, vol. 62, no. 3, pp. 227–252, 2011. [Online]. Available: https://www.sciencedirect.com/science/article/pii/S0166361510001521

[131] W. Liu, K. Huang, X. Zhou, and S. Durrani, "Next generation backscatter communication: Systems, techniques, and applications," *EURASIP J. Wireless Commun. Netw.*, vol. 2019, no. 1, pp. 1–11, 2019.

[132] V. Talla, M. Hessar, B. Kellogg, A. Najafi, J. R. Smith, and S. Gollakota, "Lora backscatter: Enabling the vision of ubiquitous connectivity," in *Proc. ACM Interactive, Mobile, Wearable, Ubiquitous Technol.*, vol. 1, no. 3, 2017, Art. no. 105.

[133] Y. Peng et al., "PLoRa: A passive long-range data network from ambient LoRa transmissions," in *Proc. Conf. ACM Special Int. Group Data Commun.*, 2018, pp. 147–160.

[134] J. Jiang, Z. Xu, F. Dang, and J. Wang, "Long-range ambient LoRa backscatter with parallel decoding," in *Proc. 27th Annu. Int. Conf. Mobile Comput. Netw.*, 2021, pp. 684–696.

[135] A. Eid, J. Hester, and M. M. Tentzeris, "A scalable high-gain and large-beamwidth mm-wave harvesting approach for 5G-powered IoT," in *Proc. IEEE MTT-S Int. Microw. Symp.*, 2019, pp. 1309–1312.

[136] J. Kimionis, A. Georgiadis, S. N. Daskalakis, and M. M. Tentzeris, "A printed millimetre-Wave modulator and antenna array for backscatter communications at gigabit data rates," *Nature Electron.*, vol. 4, no. 6, pp. 439–446, 2021.

[137] Z. Li et al., "FerroTag: A paper-based mmWave-scannable tagging infrastructure," in *Proc. ACM SenSys*, 2019, pp. 324–337. [Online]. Available: https://doi.org/10.1145/3356250.3360019

[138] R. Correia et al., "Chirp based backscatter modulation," in *Proc. IEEE MTT-S Int. Microw. Symp.*, 2019, pp. 279–282.

[139] M. Hessar, A. Najafi, and S. Gollakota, "NetScatter: Enabling large-scale backscatter networks," in *Proc. 16th USENIX Symp. Netw. Syst. Des. Implementation*, 2019, pp. 271–284. [Online]. Available: https://www.usenix.org/conference/nsdi19/presentation/hessar

[140] Z. Qin, F. Y. Li, G. Y. Li, J. A. McCann, and Q. Ni, "Low-power wide-area networks for sustainable IoT," *IEEE Wireless Commun.*, vol. 26, no. 3, pp. 140–145, Jun. 2019.

[141] S. Long and F. Miao, "Research on ZigBee wireless communication technology and its application," in *Proc. IEEE 4th Adv. Inf. Technol., Electron. Automat. Control Conf.*, 2019, vol. 1, pp. 1830–1834.

[142] C. Pon, "Retrodirective array using the heterodyne technique," *IEEE Trans. Antennas Propag.*, vol. 12, no. 2, pp. 176–180, Feb. 1964.

[143] E. Soltanaghaei et al., "Millimetro: mmWave retro-reflective tags for accurate, long range localization," in *Proc. 27th Annu. Int. Conf. Mobile Comput. Netw.*, 2021, pp. 69–82.

[144] M. H. Mazaheri, A. Chen, and O. Abari, "mmTag: A millimeter wave backscatter network," in *Proc. ACM SIGCOMM*, 2021, pp. 463–474. [Online]. Available: https://doi.org/10.1145/3452296.3472917

[145] J. G. Hester and M. M. Tentzeris, "A mm-wave ultra-long-range energy-autonomous printed RFID-enabled Van-Atta wireless sensor: At the crossroads of 5G and IoT," in *Proc. IEEE MTT-S Int. Microw. Symp.*, 2017, pp. 1557–1560.

[146] E. Sharp and M. Diab, "Van Atta reflector array," *IEEE Trans. Antennas Propag.*, vol. 8, no. 4, pp. 436–438, Jul. 1960.

[147] A. Kludze and Y. Ghasempour, "Leakyscatter: A frequency-agile directional backscatter network above 100 GHz," in *Proc. 20th USENIX Symp. Networked Syst. Design Implementation*, 2023.

[148] D. R. Jackson, C. Caloz and T. Itoh, "Leaky-wave antennas," in *Proc. IEEE*, vol. 100, no. 7, 2012, pp. 325–367, doi: 10.1109/JPROC.2012.2187410.

[149] Y. Ghasempour, C.-Y. Yeh, R. Shrestha, Y. Amarasinghe, D. Mittleman, and E. W. Knightly, "Leakytrack: Non-coherent single-antenna nodal and environmental mobility tracking with a leaky-wave antenna," in *Proc. 18th Conf. Embedded Netw. Sensor Syst.*, 2020, pp. 56–68.

[150] Y. Ghasempour, R. Shrestha, A. Charous, E. Knightly, and D. M. Mittleman, "Single-shot link discovery for terahertz wireless networks," *Nature Commun.*, vol. 11, no. 1, 2020, Art. no. 2017.

[151] A. Kludze, R. Shrestha, E. Knightly, D. Mittleman, and Y. Ghasempour, "3D localization via a single non-coherent THz antenna," in *Proc. 28th Annu. Int. Conf. Mobile Comput. Netw.*, 2022, pp. 120–132.

[152] H. Saeidi, S. Venkatesh, X. Lu, and K. Sengupta, "22.1 THz prism: One-shot simultaneous multi-node angular localization using spectrum-to-space mapping with 360-to-400 GHz broadband transceiver and dual-port integrated leaky-wave antennas," in *Proc. IEEE Int. Solid-State Circuits Conf.*, 2021, vol. 64, pp. 314–316.

[153] M. Fantuzzi, D. Masotti, and A. Costanzo, "A novel integrated UWB–UHF one-port antenna for localization and energy harvesting," *IEEE Trans. Antennas Propag.*, vol. 63, no. 9, pp. 3839–3848, Sep. 2015.

[154] A. Costanzo, D. Masotti, M. Fantuzzi, and M. D. Prete, "Co-design strategies for energy-efficient UWB and UHF wireless systems," *IEEE Trans. Microw. Theory Techn.*, vol. 65, no. 5, pp. 1852–1863, May 2017.

[155] A. Costanzo et al., "Energy autonomous UWB localization," *IEEE J. Radio Freq. Identification*, vol. 1, no. 3, pp. 228–244, Sep. 2017.

[156] S. Agarwal, D. Chadzichristodoulou, A. Quddious, D. Masotti, S. Nikolaou, and A. Costanzo, "HIS design for an environment-robust UHF/UWB antenna with 3D-printed inclusions," in *Proc. 51st Eur. Microw. Conf.*, 2022, pp. 817–820.

[157] N. Decarli, M. D. Prete, D. Masotti, D. Dardari, and A. Costanzo, "High-accuracy localization of passive tags with multisine excitations," *IEEE Trans. Microw. Theory Techn.*, vol. 66, no. 12, pp. 5894–5908, Dec. 2018.